

Unleashing the Intrinsic Visual Representation Capability of Multimodal Large Language Models

Hengzhuang Li^{♣,*} Xinsong Zhang^{♣,✉} Qiming Peng[♣] Bin Luo[♣]
 Han Hu[♣] Dengyang Jiang[♥] Han-Jia Ye[♣] Teng Zhang^{♣,✉} Hai Jin[♣]

[♣]HUST [♥]Tencent Hunyuan Research [♥]HKUST [♣]NJU
^{*}Work done at Tencent Hunyuan Research [✉]Corresponding authors

Abstract

Multimodal Large Language Models (MLLMs) have demonstrated remarkable proficiency in multimodal tasks. Despite their impressive performance, MLLMs suffer from the modality imbalance issue, where visual information is often underutilized compared to textual representations in deeper layers, leading to degraded visual performance or hallucinations. This issue stems from the predominant reliance on next-text-token-prediction during training, which fails to provide direct visual supervisory signals, resulting in progressive homogenization of visual representations throughout the layers. To this end, we propose **Latent Visual Reconstruction (LaVer)**, a novel training framework that facilitates MLLMs in learning more discriminative visual representations via masked image modeling in the joint latent semantic space of LLM. Our method offers direct visual activation to MLLMs, which exhibit increased visual attention allocation, indicating enhanced utilization of visual information. Extensive experiments across diverse benchmarks prove the superiority of our approach in various scenarios, especially those requiring dense visual capabilities. Code of LaVer is available at <https://github.com/Fir-lat/LaVer>.

1. Introduction

Multimodal Large Language Models (MLLMs) [2, 3, 7, 8, 26, 60, 66–68, 102] have emerged as a transformative paradigm for real-world multimodal tasks, fusing the linguistic reasoning power of Large Language Models (LLMs) [6, 12, 43, 86, 92, 93, 105, 119, 120] with the advanced cognition and perception abilities of vision models [87, 94, 97, 106, 126]. MLLMs have demonstrated significant potential in enhancing visual capabilities across a wide spectrum of tasks, ranging from visual question answering to complex multimodal reasoning [4, 39, 61, 130].

Despite their impressive capabilities, MLLMs are afflicted by the *modality imbalance* issue [15, 129, 134],

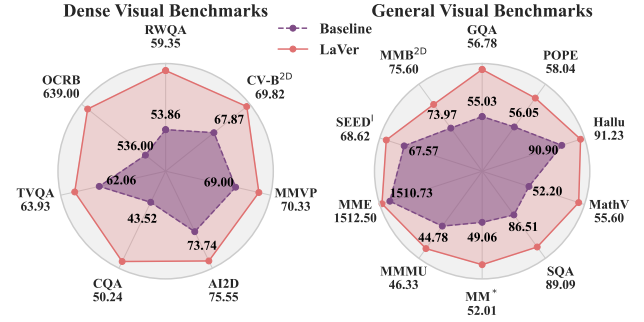


Figure 1. **Benchmark Performance.** LaVer consistently outperforms the baseline across diverse benchmarks, especially on dense visual tasks such as OCRB [71] and CQA [78]. The results are obtained with SigLIP 2 [106] and Qwen2.5-7B-Instruct [91].

where the model exhibits a systematic bias towards textual information in multimodal tasks. MLLMs frequently generate confident responses even when presented with absent or incongruent visual inputs, as empirically demonstrated in [73, 88, 129, 134]. When rich visual information is available, MLLMs still tend to produce outputs predominantly grounded in textual context [51, 57]. Qualitative analysis reveals that MLLMs allocate substantially more attention to textual content than vision tokens [117], as the text modality demonstrably contributing more to the predictions [88].

The consequences of this modality imbalance are multifaceted. Model outputs become systematically biased toward the dominant textual modality, fundamentally failing to leverage the full potential of underrepresented visual information [95, 110], leading to degraded performance across various benchmarks [69, 90, 134] and increased visual hallucinations [44, 57, 58, 96, 114], ultimately diminishing the reliability [73, 103] of MLLMs. Addressing this challenge is crucial, as ideal MLLMs should seamlessly integrate and leverage the full potential of each modality to achieve robust multimodal understanding [22, 103].

The modality imbalance stems from the fundamental asymmetry of MLLM’s training paradigm: supervision signals are derived exclusively by *next-text-token-*

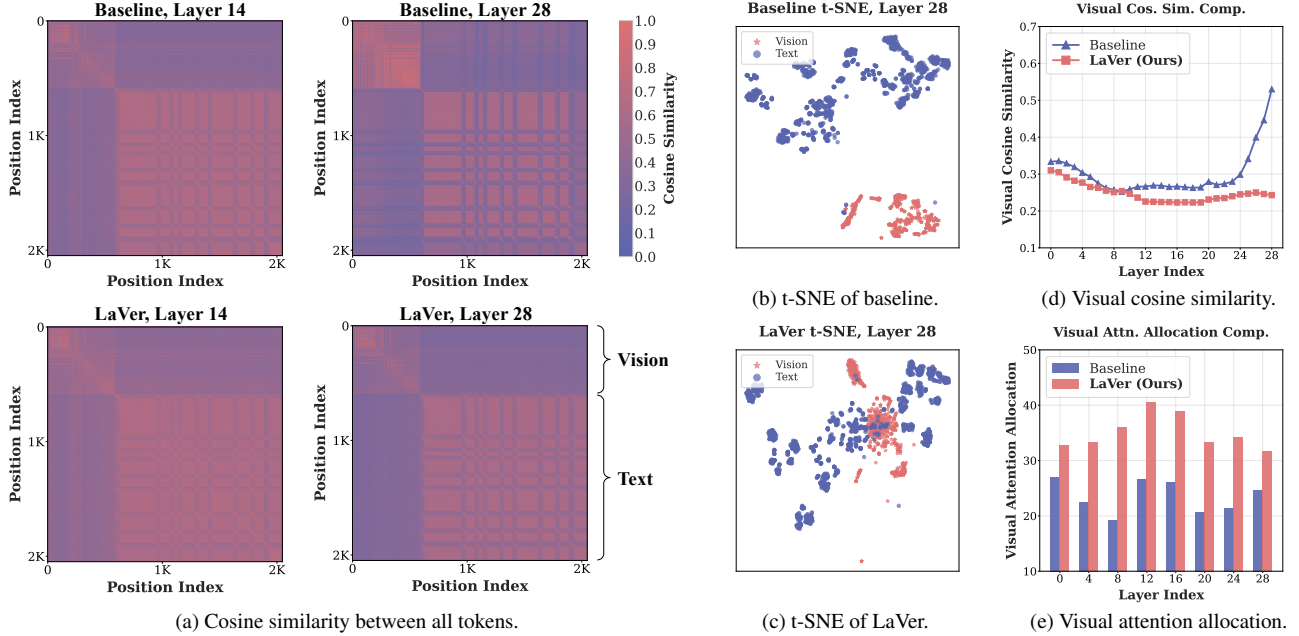


Figure 2. **Progressive visual representation homogenization.** (a) presents higher feature cosine similarities of the last layer than middle layer. (b-c) display the t-SNE visualizations of the output embeddings. (d) quantifies the averaged vision cosine similarity. (e) quantifies the allocated attention score for vision tokens. LaVer outputs discriminative visual representations with higher attention allocation. The quantitative results are obtained with SigLIP 2 [106] and Qwen2.5-7B-Instruct [91], averaged across the images from MMVP [103].

prediction [111, 112, 138], while visual modeling largely depend on implicit vision-to-text alignment [77, 102, 103], thereby providing indirect and weaker supervision signals for the model’s intrinsic visual representation [103, 112]. This asymmetric supervision naturally biases the model toward prioritizing textual information and discarding visual information that is not meaningful for text outputs, particularly given the LLM backbone’s dominant language capability [134], which is trained on large-scale corpora [91].

We further provide empirical validation of modality imbalance by revealing the *progressive visual representation homogenization* in Fig. 2. We observe that visual tokens exhibit significant deterioration in deeper layers, characterized by drastically enlarged token-wise cosine similarity shown in Fig. 2a and Fig. 2d. Besides, t-SNE visualization in Fig. 2b demonstrates that vision tokens remain significantly separated from text tokens in the output space. This homogenization pattern indicates substantial visual information loss as representations propagate through the model, which aligns with prior findings that MLLMs generate increasingly aligned yet less informative visual representations in deeper layers [109], and that vision-text information flow occurs predominantly in the early layers [52, 122, 128]. This evidence underscores the fundamental limitations in MLLMs’ *intrinsic visual representation capability*.

To this end, we propose **Latent Visual Reconstruction (LaVer)** to enhance the intrinsic visual modeling capability of MLLMs by learning discriminative multimodal rep-

resentations within the joint high-level semantic space of LLMs. Technically, we employ the *Masked Image Modeling (MIM)* paradigm [9, 42, 46, 104, 136], capitalizing the spatial redundancy of natural visual signals [46, 128, 136]. Different from previous techniques that apply masks to raw pixels [42, 46] or require reconstruction of fine-grained visual signals [112], we randomly mask vision tokens in the input embedding space and train the model to recover the masked tokens in the latent space of LLM, thereby providing direct intrinsic supervision for visual representations. Our method concurrently shapes the model’s latent semantic space for all modalities by learning to predict the missing vision token and the next text token. LaVer inhibits the homogenization of vision tokens in deeper layers (Fig. 2a and Fig. 2d), generates more unified multimodal representations (Fig. 2c), and consistently increases the visual attention allocation (Fig. 2e), indicating more comprehensive utilization of visual information. Furthermore, we propose *Clipped Gram-Anchoring* to prevent the model from hacking MIM by outputting identical visual embeddings.

Empirical analysis demonstrates that LaVer achieves competitive performance across a wide suite of multimodal benchmarks, especially for dense visual tasks [71, 78, 98, 102, 103] that require comprehensive visual information utilization, e.g., 19.22% improvement on OCRB [71], shown in Fig. 1. The unleashed visual representations also facilitate sophisticated visual reasoning capabilities, such as reasoning segmentation where precise visual un-

derstanding must be tightly coupled with language instructions [55, 101]. These results validate that our approach enables more effective multimodal learning that provides unified representations for all modalities. The primary contributions of this work are summarized as follows.

- We investigate self-supervised paradigm for MLLMs and propose **LaVer**, a novel multimodal training framework that derives direct visual supervisory signals by reconstructing the masked vision token in the latent space.
- We further validate the modality imbalance problem by revealing the progressive homogenization of visual features in deeper layers of MLLMs.
- We conduct extensive empirical analysis to validate that LaVer can consistently improve multimodal understanding, especially on dense visual tasks.

2. Related Works

2.1. Multimodal Large Language Models

Recent advancements in LLMs [6, 11, 27, 86, 105, 119, 120] and vision models [17, 87, 94, 97, 106, 126] have catalyzed the rapid evolution of MLLMs [2, 3, 7, 8, 26, 60, 62, 66–68, 102]. The typical paradigm for these models is a plug-in architecture [3, 67], which incorporates a visual encoder to convert images into visual features, a connector (e.g., an MLP [67]) to map these features into the input embedding space of LLM, and a pretrained LLM that integrates the visual information to execute multimodal tasks. MLLMs can be boosted by scaling data [3, 8], powerful LLMs [43, 120], and advanced ViTs [28, 38, 91]. However, the *next-text-token-prediction* potentially hinders MLLMs from developing intrinsic visual modeling capacities.

2.2. Vision-enhanced MLLMs

Numerous initiatives have been undertaken to mitigate the modality imbalance [15, 129, 134] and improve the visual understanding of MLLMs for complex tasks [102, 127, 130]. These include curating robust, modality-balanced datasets for evaluation and training [20, 22, 88], prompting strategies to encourage visual utilization [69], and visual contrastive decoding techniques to mitigate textual overreliance [45, 84]. Reinforcement learning-based approaches further enhance vision-centric optimization [64, 73, 89, 131], while alternative strategies enrich visual inputs via additional expert modules [24, 60, 74, 102, 103, 121, 123], advanced projector routing [79, 115], or fusion strategies [16, 65]. Methods focusing on intrinsic visual modeling have also gained attention, including directly allocating greater attention to vision tokens [69, 131] and employing visual reconstruction objectives to retain the fine-grained visual information [111, 112, 118], being potentially impeded by redundancy and noise in low-level pixels [82], thus suboptimal for tasks requiring high-level semantic rea-

soning [81]. In contrast to these methods, LaVer predicts the masked vision tokens in the same latent space of LLM, thus producing more unified multimodal representations.

2.3. Masked Image Modeling

Masked Image Modeling (MIM) [9, 46, 104, 136] has emerged as a cornerstone of self-supervised learning [33, 41], deriving powerful supervisory signals via pretext tasks. Early approaches explored predicting contextual relationships within images [32, 80, 85]. Recent advances focus on reconstructing masked image patches: BEiT [9] and DAVINCI [31] reconstruct discrete vision tokens from VQ-VAE [36], iBOT [136] employs an online teacher to provide visual targets, MAE [46] demonstrates the effectiveness of pixel-space reconstruction, and JEPA [5, 10] formalizes prediction within a learned latent space. Extensions to multimodal scenarios [19, 40, 132] foster learning unified multimodal representations. However, MLLMs haven’t fully leveraged this paradigm. This study explores enhancing the intrinsic visual modeling capability of MLLMs by forcing them to reconstruct latent visual representations.

3. Preliminaries

Multimodal Large Language Models. Denote the LLM backbone as \mathcal{F}_θ , parameterized by θ , modeling the canonical causal distribution $p_\theta(\mathbf{x}) = \prod_{i=1}^T p_\theta(\mathbf{x}_i | \mathbf{x}_{<i})$ with respect to each text token \mathbf{x}_i , where $\{\mathbf{x}_i\}_{i=1}^T$ denotes the sequence of text tokens and T denotes the sequence length. Typical MLLMs [3, 66, 67] adopt the cascade-style architecture. Specifically, the image $\mathbf{I} \in \mathbb{R}^{H \times W \times 3}$ (H and W denote the height and width respectively) is first encoded into visual features by a ξ -parameterized visual encoder \mathcal{G}_ξ and then projected into vision tokens $\mathbf{V} = \{\mathbf{v}_1, \dots, \mathbf{v}_N\} \in \mathbb{R}^{N \times D}$ by a ϕ -parameterized connector \mathcal{H}_ϕ , where N denotes the length of vision token sequence and D denotes the hidden dimension of the LLM. The canonical causal distribution for a multimodal sequence is formulated as:

$$p_\Theta(\mathbf{x}) = \prod_{i=1}^T p_\Theta(\mathbf{x}_i | \mathbf{x}_{<i}, \mathbf{V}), \mathbf{V} = \mathcal{H}_\phi \circ \mathcal{G}_\xi(\mathbf{I}), \quad (1)$$

where $\Theta = \{\theta, \xi, \phi\}$ denotes the parameters. The visual encoder could be pretrained vision models [8, 17, 29, 38, 87, 94, 97, 106, 126] or even a simple MLP which projects raw pixel patches into vision tokens directly [23, 30, 56].

Training paradigm for MLLMs. Typical MLLMs derive supervision by solely maximizing the log-likelihood of the text responses. The learning objective is formulated as Cross-Entropy loss over the text vocabulary as follows:

$$\mathcal{L}_{\text{LM}}(\Theta; \mathbf{I}, \mathbf{x}) = -\frac{1}{T-P} \sum_{i=P+1}^T \log p_\Theta(\mathbf{x}_i | \mathbf{x}_{<i}, \mathbf{V}), \quad (2)$$

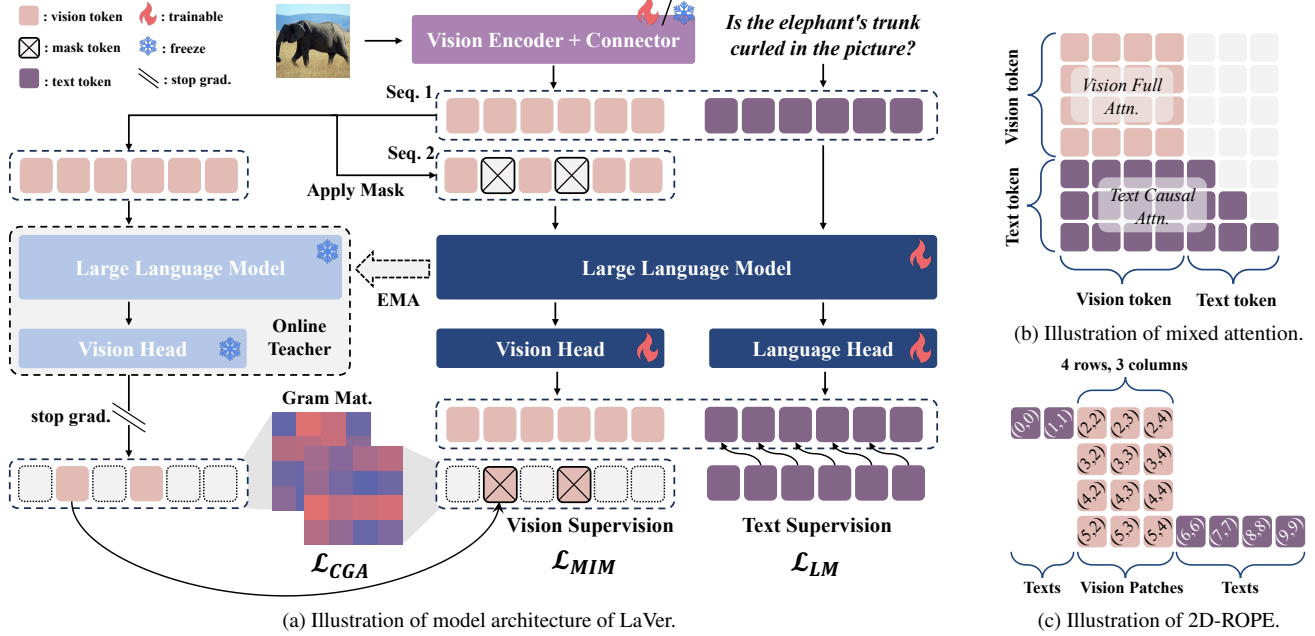


Figure 3. **Overview of LaVer.** (a) depicts the student-teacher framework where the MLLM is trained to predict the teacher’s visual output embeddings for the masked positions, regularized by the Clipped Gram-Anchoring to prevent feature inconsistency. (b) depicts the mixed attention mechanism. (c) depicts the 2D-ROPE mechanism. LaVer learns discriminative visual representations by self-supervised MIM.

where P denotes prompt length (i.e., the prefix vision tokens and instruction tokens). Following LLaVA-OneVision 1.5 [3], we adopt a three-stage training receipt (Sec. 5.1).

4. Methodology

This section elucidates how LaVer encourages MLLMs to learn discriminative visual representations, as depicted in Fig. 3. As shown in Fig. 2, *progressive visual feature homogenization* indicates that MLLMs gradually discard meaningful visual semantics, utilizing only partial visual information for multimodal tasks. To address this limitation, we force MLLMs to maintain visual structural information via masked image modeling, requiring the model to restore the missing visual information based on the visual context (Sec. 4.1). This process strengthens the model’s intrinsic visual perception ability. Nonetheless, models may exploit this objective by producing highly identical visual features for all vision tokens. Consequently, we introduce a regularizer to avert this shortcut (Sec. 4.2).

4.1. Latent Visual Reconstruction

Masking. We encode an image I into visual features $V = \mathcal{H}_\phi \circ \mathcal{G}_\xi(I) \in \mathbb{R}^{N \times D}$. A binary mask $\mathcal{M} \in \{0, 1\}^N$ is generated by randomly selecting a subset of vision positions at probability r (mask ratio), where $\mathcal{M}_i = 1$ indicates the i -th token is masked. The masked vision tokens \tilde{V} are constructed by replacing the original features at masked positions with a learned mask token $e_{[\text{MASK}]} \in \mathbb{R}^D$: $\tilde{v}_i = \mathcal{M}_i \cdot e_{[\text{MASK}]} + (1 - \mathcal{M}_i) \cdot v_i$ for $i = 1, \dots, N$. $e_{[\text{MASK}]}$

is learned along with the LLM’s word embeddings.

Vision head architecture. We employ a 3-layer multi-layer perceptron (MLP) as the vision head to project the visual output embeddings into visual logits, following [136]. Let $\tilde{H} = \{\tilde{h}_1, \dots, \tilde{h}_N\} \in \mathbb{R}^{N \times D}$ denote the hidden state corresponding to the vision tokens \tilde{V} , derived by $\tilde{H} = \mathcal{F}_\theta(\tilde{V})$. The vision head \mathcal{V}_ψ with parameters ψ transforms this representation through the MLP with ReLU activations between layers. Formally, the transformation is defined as:

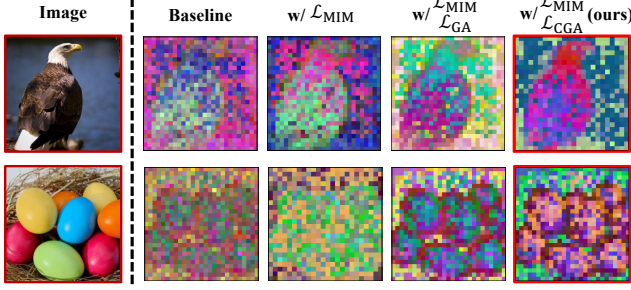
$$\tilde{Z} = \mathcal{V}_\psi(\tilde{H}), \quad (3)$$

where $\tilde{Z} = \{\tilde{z}_1, \dots, \tilde{z}_N\} \in \mathbb{R}^{N \times D_v}$ denotes the visual logits, and D_v denotes the dimension of the visual logits.

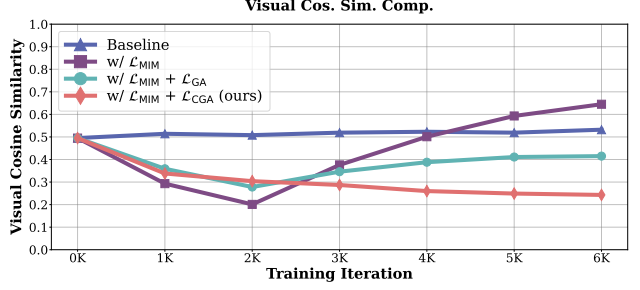
Training paradigm. We employ a student-teacher framework where MLLMs are encouraged to predict the teacher’s visual embeddings for the masked vision positions [136]. The teacher model $\hat{\Phi} = \{\hat{\theta}, \hat{\psi}\}$ is maintained as an exponential moving average (EMA) of the student model $\Phi = \{\theta, \psi\}$ over training iterations. The teacher model processes the original unmasked vision tokens V to generate target visual logits $\hat{Z} = \{\hat{z}_1, \dots, \hat{z}_N\} \in \mathbb{R}^{N \times D_v}$ for the same positions, i.e., $\hat{Z} = \mathcal{V}_{\hat{\psi}} \circ \mathcal{F}_{\hat{\theta}}(V)$. At updating step t , the teacher parameters are updated as:

$$\begin{aligned} \hat{\theta}^{(t)} &= \lambda \hat{\theta}^{(t-1)} + (1 - \lambda) \theta^{(t)}, \\ \hat{\psi}^{(t)} &= \lambda \hat{\psi}^{(t-1)} + (1 - \lambda) \psi^{(t)}, \end{aligned} \quad (4)$$

where $\lambda \in [0, 1]$ is the EMA decay rate.



(a) PCA visualization of visual features.



(b) Averaged cosine similarity between vision tokens.

Figure 4. **Effects of MIM on visual feature consistency.** (a) illustrates PCA visualization of visual features with different components. (b) illustrates the averaged cosine similarity between vision tokens along training. Our method displays the most discriminative features.

Ideally, the student model Φ should be able to restore the masked vision tokens via the visual contextual information by leveraging the visual redundancy [46], maintaining discriminative visual structural representations. Specifically, the distribution of the predicted visual logits \tilde{Z} should be close to the distribution of the target visual logits \hat{Z} that comes from clean representation process of the teacher $\hat{\Phi}$.

Learning objective. The student model Φ is optimized to minimize the cross-entropy between its prediction \tilde{z} and the teacher’s target \hat{z} for masked positions, encouraging the student to reconstruct the high-level visual structural information. Formally, the MIM loss function is formalized as:

$$\mathcal{L}_{\text{MIM}} = - \sum_{i \in \mathcal{P}_{\mathcal{M}}} \text{softmax}(\hat{z}_i / \tau_{\text{tea.}}) \cdot \log \text{softmax}(\tilde{z}_i / \tau_{\text{stu.}}), \quad (5)$$

where $\mathcal{P}_{\mathcal{M}} = \{i \in \{1, \dots, N\} \mid \mathcal{M}_i = 1\}$ denotes the set of indices corresponding to the masked positions, $\tau_{\text{tea.}} > 0$ and $\tau_{\text{stu.}} > 0$ are temperature scalars that control the sharpness of the softmax distribution for \hat{z} and \tilde{z} , respectively.

Improving Spatial Awareness. MIM inherently requires the model to leverage spatial contextual information from neighboring regions to accurately reconstruct masked vision tokens [9, 46, 136], meaning that vision tokens need to attend to the entire image to effectively capture global spatial visual semantics [34, 72]. Nonetheless, the standard causal attention mechanism [6, 108] and the Rotary Position Embedding (RoPE) [99, 105], which are designed primarily for sequential text processing, are fundamentally misaligned with the demands of visual modeling. Subsequently, we introduce the mixed attention mechanism [18, 56, 94, 126], which constructs bidirectional full attention for vision tokens and causal attention for text tokens (Fig. 3b). We also adopt 2D-RoPE [8, 48, 113] to better exploit the spatial structure of visual information by treating the image patch grid coordinates as positional index pairs for vision tokens (Fig. 3c). The compatibility with the sequential processing of textual data is ensured by assigning identical row and column indices for text tokens.

Independent Reconstruction. To ensure independent visual reconstruction without interfering with the original

learning paradigm, we leave the original multimodal sequence intact, and pack all the masked vision tokens to form a separate new sequence (Fig. 3a). We adopt the diagonally blocked bidirectional attention and blocked 2D-RoPE to prevent information leakage between different images.

4.2. Mitigating Visual Feature Inconsistency

Visual Feature Inconsistency. We observe that learning solely via MIM induces *visual feature inconsistency*, wherein vision tokens exhibit high cosine similarities despite containing substantially different visual semantics, similar to observations in [37, 87, 97]. This phenomenon is illustrated in Fig. 4a, where visual features become entangled, leading to collapsed local visual structural information. As shown in Fig. 4b, the averaged cosine similarity during training reveals that MIM alone causes similarity to decrease rapidly in early stages but ultimately converges to values exceeding the baseline. This behavior indicates that without proper regularization, visual features can freely drift and hack the MIM loss. The underlying cause is that the loss function in Eqn. (5) only enforces token-wise distribution matching between student and teacher for individual masked tokens, while failing to preserve the structural diversity across the entire set of vision tokens.

Gram-Anchoring. To mitigate visual feature inconsistency, we explore the *Gram-Anchoring* (GA) mechanism [97] that enforces the relative structure of visual features from student to match the teacher’s while making the features free to move. Specifically, the Gram matrices $G \in \mathbb{R}^{N \times N}$ for visual logits Z is calculated as follows:

$$G(Z) = \text{Norm}(Z) \cdot \text{Norm}(Z)^\top, Z \in \mathbb{R}^{N \times D_v}, \quad (6)$$

where $\text{Norm}(\cdot) = \cdot / \|\cdot\|$ denotes the L_2 -normalization along the feature dimension. The GA loss is then formulated as:

$$\mathcal{L}_{\text{GA}} = \|G(\tilde{Z}) - G(\hat{Z})\|_F^2. \quad (7)$$

Clipped Gram-Anchoring. While GA effectively mitigates visual feature inconsistency through structural similarity preservation, it exhibits limited capacity for learning discriminative representations. As evidenced in Fig. 4b,

Table 1. **Main results on various benchmarks with varied MLLM architectures.** (%) We adopt the VLMEvalKit [35] toolboxes to conduct the evaluation, following the official guideline to implement the missing benchmarks. LaVer consistently outperforms the baseline across most benchmarks, especially on benchmarks that require dense visual capabilities, including the OCR and vision-centric tasks.

Benchmark		Fixed-Resolution Visual Encoder									Native-Resolution Encoder						Encoder-Free		
		SigLIP2			CLIP			DINOv2			AIMv2			Qwen-ViT			MLP + Qwen 2.5		
		Baseline	LaVer	Δ_{Baseline}	Baseline	LaVer	Δ_{Baseline}	Baseline	LaVer	Δ_{Baseline}	Baseline	LaVer	Δ_{Baseline}	Baseline	LaVer	Δ_{Baseline}	Baseline	LaVer	Δ_{Baseline}
General VQA	GQA [49]	55.03	56.78	$\uparrow 1.75$	51.51	54.77	$\uparrow 3.26$	49.25	53.02	$\uparrow 3.77$	53.02	57.04	$\uparrow 4.02$	56.78	56.78	$\uparrow 0.00$	33.17	32.91	$\downarrow 0.26$
	MMB ^{EN} [70]	73.97	75.60	$\uparrow 1.63$	68.64	69.93	$\uparrow 1.29$	59.19	61.68	$\uparrow 2.49$	74.14	75.43	$\uparrow 1.29$	77.66	79.04	$\uparrow 1.38$	26.80	29.04	$\uparrow 2.24$
	SEED ^I [59]	67.57	68.62	$\uparrow 1.05$	64.36	65.20	$\uparrow 0.84$	62.24	62.98	$\uparrow 0.74$	66.96	67.04	$\uparrow 0.08$	62.93	61.95	$\downarrow 0.98$	40.62	43.70	$\uparrow 3.08$
	MME [39]	1510.73	1512.50	$\uparrow 1.77$	1289.62	1474.65	$\uparrow 185.03$	1166.51	1275.04	$\uparrow 108.53$	1485.48	1446.67	$\downarrow 38.81$	1556.08	1592.90	$\uparrow 36.82$	1014.05	1138.67	$\uparrow 124.62$
	RWQA [25]	53.86	59.35	$\uparrow 5.49$	54.25	56.47	$\uparrow 2.22$	49.41	53.73	$\uparrow 4.32$	56.21	57.78	$\uparrow 1.57$	55.05	58.17	$\uparrow 3.12$	44.18	48.76	$\uparrow 4.58$
	MMMU [125]	44.78	46.33	$\uparrow 1.55$	44.56	44.56	$\uparrow 0.00$	42.24	42.44	$\uparrow 0.20$	44.56	45.00	$\uparrow 0.44$	45.67	47.56	$\uparrow 1.89$	39.78	40.67	$\uparrow 0.89$
	MM* [20]	49.06	52.01	$\uparrow 2.95$	43.17	45.45	$\uparrow 2.28$	39.49	41.16	$\uparrow 1.67$	47.52	49.80	$\uparrow 2.28$	53.82	54.62	$\uparrow 0.80$	30.99	31.99	$\uparrow 1.00$
OCR VQA	OCRB [71]	536	639	$\uparrow 1103$	306	365	$\uparrow 59$	317	384	$\uparrow 67$	399	412	$\uparrow 13$	813	815	$\uparrow 2$	144	153	$\uparrow 9$
	TVQA [98]	67.87	69.82	$\uparrow 1.95$	64.39	65.58	$\uparrow 1.19$	60.08	61.34	$\uparrow 1.26$	63.70	67.04	$\uparrow 3.34$	62.87	69.89	$\uparrow 7.02$	52.29	54.67	$\uparrow 2.38$
	CQA [78]	62.06	63.93	$\uparrow 1.87$	43.86	49.93	$\uparrow 6.07$	41.91	42.47	$\uparrow 0.56$	61.06	61.78	$\uparrow 0.72$	72.01	74.55	$\uparrow 2.54$	10.56	11.28	$\uparrow 0.72$
	AI2D [53]	86.51	89.09	$\uparrow 2.58$	81.61	83.30	$\uparrow 1.69$	75.71	78.28	$\uparrow 2.57$	86.02	87.46	$\uparrow 1.44$	88.00	92.71	$\uparrow 4.71$	74.17	76.28	$\uparrow 2.11$
Vision-Centric	MMVP [103]	43.52	50.24	$\uparrow 6.72$	27.36	39.36	$\uparrow 12.00$	28.48	28.64	$\uparrow 0.16$	35.28	37.68	$\uparrow 2.40$	63.52	65.20	$\uparrow 1.68$	18.08	19.04	$\uparrow 0.96$
	CV-B ^{2D} [102]	52.20	55.60	$\uparrow 3.40$	45.40	48.90	$\uparrow 3.50$	42.10	44.90	$\uparrow 2.80$	50.60	51.10	$\uparrow 0.50$	59.90	61.60	$\uparrow 1.70$	37.40	38.00	$\uparrow 0.60$
Math & Know.	SQA [75]	73.74	75.55	$\uparrow 1.81$	66.00	70.40	$\uparrow 4.40$	65.67	65.87	$\uparrow 0.20$	73.15	73.80	$\uparrow 0.65$	76.36	77.53	$\uparrow 1.17$	60.33	63.20	$\uparrow 2.87$
	MathV [76]	56.05	58.04	$\uparrow 1.99$	53.42	55.95	$\uparrow 2.53$	47.73	48.26	$\uparrow 0.53$	56.05	56.31	$\uparrow 0.26$	57.10	62.36	$\uparrow 5.26$	46.48	46.37	$\downarrow 0.11$
Hallucination	Hallu [44]	69.00	70.33	$\uparrow 1.33$	60.00	64.00	$\uparrow 4.00$	62.00	62.67	$\uparrow 0.67$	74.33	75.00	$\uparrow 0.67$	63.00	66.00	$\uparrow 3.00$	52.00	53.00	$\uparrow 1.00$
	POPE [63]	90.90	91.23	$\uparrow 0.33$	90.50	90.30	$\downarrow 0.20$	88.30	88.53	$\uparrow 0.23$	86.27	86.37	$\uparrow 0.10$	89.10	89.57	$\uparrow 0.47$	50.93	52.03	$\uparrow 1.10$
Average		55.72	57.87	$\uparrow 2.15$	50.58	53.24	$\uparrow 2.66$	47.92	49.23	$\uparrow 1.31$	54.70	55.86	$\uparrow 1.16$	57.96	59.94	$\uparrow 1.99$	36.37	37.74	$\uparrow 1.37$

cosine similarity initially decreases but gradually increases during training, revealing that GA inadequately penalizes feature inconsistency. This limitation stems from the symmetric nature of Eqn. (7), which equally penalizes all deviations between teacher and student Gram matrices irrespective of deviation direction. Critically, when $G(\tilde{Z}) < G(\hat{Z})$, indicating the student produces more discriminative features than the teacher, Eqn. (7) inadvertently suppresses this desirable behavior. We therefore introduce asymmetric *Clipped Gram-Anchoring* (CGA):

$$\mathcal{L}_{\text{CGA}} = \|\text{Clip}(G(\tilde{Z}) - G(\hat{Z}))\|_F^2, \quad (8)$$

where $\text{Clip}(\cdot) = \max(0, \cdot)$ denotes element-wise clipping. CGA selectively penalizes only undesirable deviations where student features become less discriminative than the teacher, thereby encouraging the development of superior representations. CGA consistently yields discriminative features with decreasing cosine similarity (Fig. 4b).

Final objective. The objective for our LaVer is to jointly minimize the sum of the LM, the MIM, and the CGA loss:

$$\mathcal{L}_{\text{Laver}} = \mathcal{L}_{\text{LM}} + \omega_{\text{MIM}}\mathcal{L}_{\text{MIM}} + \omega_{\text{CGA}}\mathcal{L}_{\text{CGA}}, \quad (9)$$

where ω_{MIM} and ω_{CGA} are trade-off parameters default to 1.0. This formulation integrates the MIM loss for visual reconstruction and the clipped gram-anchoring loss for feature diversity preservation, ensuring that the model learns both discriminative visual representations and semantic consistency across different vision tokens.

5. Experiments

5.1. Experimental Setup

Implementation Details. We employ Qwen2.5-7B-Instruct [91] as the language model backbone. To comprehensively evaluate LaVer across diverse visual

encoding paradigms, we experiment with multiple vision encoders: fixed-resolution encoders (SigLIP 2-ViT-SO400M/14@384 [106], CLIP-ViT-L/14@336 [94], DINOv2-Large/14@224 [87]), native-resolution encoders (AIMv2-Large/14 [38], Qwen-ViT from Qwen2.5-VL-7B-Instruct [8]), and an encoder-free architecture employing a single MLP to project raw pixels directly into vision tokens [23, 56]. All experiments are conducted on 16 NVIDIA A100 (80GB) GPUs. Additional implementation details are provided in the supplementary material.

Training Recipe. Following LLaVA-OneVision 1.5 [3], we adopt a three-stage training procedure to progressively develop multimodal capabilities. Stage 1 performs connector initialization for vision-language alignment using LLaVA-558K [67]. Stage 2 applies LaVer for intrinsic visual modeling and knowledge injection, learning discriminative representations from 800K pairs subsampled from FineVision 23M [116]. Stage 3 conducts visual instruction tuning [67] using 800K samples from LLaVA-OneVision 4M [60]. More settings are in the supplementary material.

Evaluation. We conduct comprehensive evaluations across diverse multimodal understanding benchmarks using VLMEvalKit [35]. Our evaluation suite encompasses (1) general VQA benchmarks: GQA [49], MMBench (MMB^{EN}) [70], SEED-Image (SEED^I) [59], MME [39], RealWorldQA (RWQA) [25], MMMU [125], and MMStar (MM*) [20]; (2) OCR benchmarks: OCRBench (OCRB) [71], TextVQA (TVQA) [98], ChartQA (CQA) [78], and AI2D [53]; (3) vision-centric benchmarks: CV-Bench-2D (CV-B^{2D}) [102] and MMVP [103]; (4) knowledge and math benchmarks: ScienceQA (SQA) [75] and MathVista (MathV) [76]; and (5) hallucination benchmarks: HallucinationBench (Hallu) [44] and POPE [63]. Average scores are computed across all benchmarks, with MME [39] and OCRB [71] normalized to [0.0, 1.0]. Evaluation details are in the supplementary material.

Table 2. **Performance on complex visual task and ablation studies on spatial awareness and loss components.** (%) (a) Performance on complex visual task. (b) Ablation study on spatial awareness. (c) Ablation study on loss components.

(a) Performance on complex visual task					(b) Ablation study on spatial awareness					(c) Ablation study on loss components				
Methods		ReasonSeg			LaVer	Mixed Attn.	2D-RoPE	SigLIP 2	CLIP	w/ \mathcal{L}_{MIM}	w/ \mathcal{L}_{GA}	w/ \mathcal{L}_{CGA}	SigLIP 2	CLIP
		Short	Long	Overall										
SigLIP 2	Baseline	38.25	52.76	51.53	✗	✗	✗	55.72	50.58	✗	✗	✗	55.72	50.58
	LaVer	39.21	53.63	52.89	✗	✓	✗	56.78	51.40	✗	✗	✗	53.76	49.71
CLIP	Baseline	35.07	50.80	48.26	✗	✗	✓	55.57	50.59	✓	✗	✗	56.46	52.01
	LaVer	37.98	52.11	49.43	✗	✓	✓	56.43	51.99	✓	✓	✓	57.87	53.24
					✓	✓	✓	57.87	53.24	✓	✗	✓	57.87	53.24

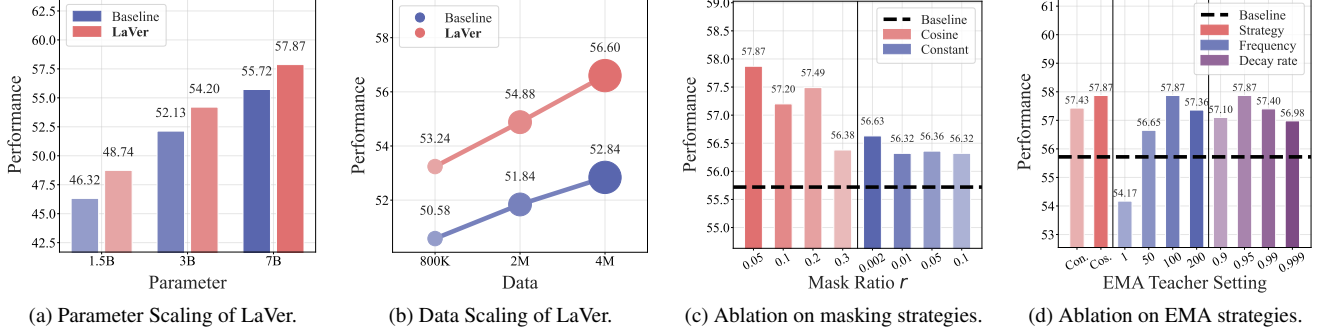


Figure 5. **Scaling properties & Ablation studies.** (a) Parameter Scaling of LaVer. (b) Data Scaling of LaVer. (c) Ablation on masking strategies. (d) Ablation on EMA updating strategies. LaVer displays significant scaling properties and robustness of hyperparameters.

5.2. Main Results

Consistent improvements across diverse vision encoders. Table 1 demonstrates that LaVer consistently outperforms baselines across nearly all benchmarks, with particularly pronounced gains on tasks requiring dense visual information comprehension, such as OCR [71, 78] and vision-centric benchmarks [102, 103]. With SigLIP 2, LaVer achieves remarkable improvements of **103 points (19.22%)** on OCR-Bench [71] and **6.72%** on MMVP [103]. CLIP exhibits similar substantial gains: **6.07%** on ChartQA [78] and **12.00%** on MMVP. Native-resolution encoders also demonstrate significant enhancements, with AIMv2 and Qwen-ViT achieving **3.34%** and **7.02%** improvements on TextVQA [98], respectively. Even the encoder-free architecture, i.e., employing a single MLP to project raw pixels into visual tokens, yields consistent **1.37%** overall gains. These improvements across diverse architectures validate LaVer’s effectiveness in enhancing discriminative visual representations within the model’s latent space, without imposing architectural constraints. Additional results are provided in the supplementary material.

Effectiveness on complex visual reasoning tasks. To further assess LaVer’s capabilities, we examine its performance on *Reasoning Segmentation* (ReasonSeg) [55], a challenging task requiring MLLMs to amalgamate language reasoning with integrated visual perception. In accordance with [101], we initialize both baseline and LaVer models from stage-2 checkpoints and fine-tune them on segmentation datasets [13, 14, 83, 124, 135] combined with LLaVA-665K [66]. Zero-shot evaluation on the test set [55, 101] re-

veals that LaVer-initialized model consistently outperforms its baseline counterpart, achieving improvements of **1.36 %** and **1.17 %** on gIoU with SigLIP 2 and CLIP, respectively (Table 2(a)). These gains demonstrate LaVer’s power to integrate visual perception with language reasoning, particularly benefiting tasks requiring sophisticated cross-modal coordination. See details in supplementary material.

Scalability of LaVer. We investigate LaVer’s scaling properties across both model and data dimensions. For parameter scaling, we evaluate Qwen2.5-Instruct [91] models at 1.5B, 3B, and 7B parameters with SigLIP 2 and CLIP, maintaining consistent training data as specified in Sec. 5.1. As shown in Fig. 5a, LaVer consistently outperforms the baseline across all model sizes with SigLIP 2, demonstrating robust scalability. For data scaling, we vary stage-2 training volume where LaVer is applied, while fixing stages 1 and 3, uniformly subsampling 800K, 2M, and 4M samples from FineVision 23M [116] and training for one epoch at each scale using Qwen2.5-7B-Instruct with SigLIP 2 and CLIP. Fig. 5b presents averaged results with CLIP, revealing that LaVer maintains substantial gains across all data scales, confirming its effectiveness under diverse training regimes. Complete results appear in the supplementary material.

5.3. Ablation Studies

Ablation on masking strategies. We examine two masking schedules: *constant*, fixing r throughout training, and *cosine*, gradually increasing r from 0.0 to the target value following a cosine schedule. Fig. 5c presents results with SigLIP 2. We find that even modest mask ratios (e.g., $r = 0.05$) yield substantial improvements, while higher ra-

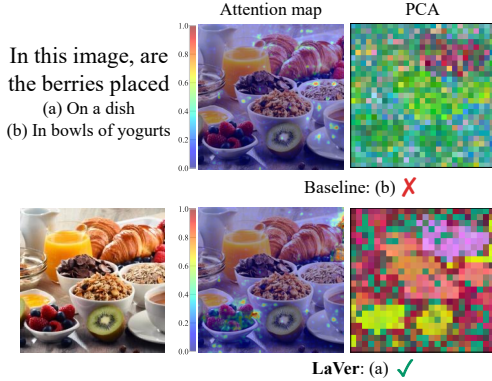


Figure 6. **Qualitative comparison.** LaVer allocates higher attention values with specific focus on corresponding visual regions, with more discriminative visual representations.

tions under cosine scheduling degrade performance, suggesting that higher ratios may require longer training process to converge effectively, as MIM-based models [17, 87, 97] typically require extensive pretraining to manifest emergent properties. The cosine schedule consistently outperforms constant scheduling, as the latter either limits reconstruction capacity or imposes excessive cold-start with fixed r . Notably, LaVer surpasses the baseline across all configurations, demonstrating robustness to masking strategies.

Ablation on EMA teacher updating strategies. We examine EMA updating strategies using SigLIP 2 in Fig. 5d. We compare two decay schedules: *constant*, fixing λ , and *cosine*, gradually increasing λ to 1.0. The cosine schedule marginally outperforms constant scheduling, with both substantially surpassing the baseline, confirming robustness across strategies. For update frequency, excessively frequent updates (every step) degrade performance, likely because rapid teacher updates destabilize learning by propagating feature inconsistencies inadvertently. Optimal performance emerges at approximately 100-step intervals (0.02 frequency over 6K iterations). Varying decay rates reveals $\lambda = 0.95$ as optimal, with all configurations outperforming the baseline. Full results are in the supplementary material.

Ablation on spatial awareness. Table 2(b) examines spatial awareness components, i.e., mixed attention and 2D-RoPE, with averaged results. Mixed attention alone improves over the baseline (56.78% vs. 55.72% for SigLIP 2) but underperforms full LaVer (57.87%), demonstrating that LaVer’s gains stem from enhanced visual representation learning rather than merely attending to all vision tokens. 2D-RoPE exhibits minimal impact (55.57% for SigLIP 2), potentially requiring longer training to realize its benefits. The complete LaVer framework consistently surpasses all ablated variants, confirming that spatial awareness components effectively complement the core methodology.

Ablation on loss components. Table 2(c) dissects the contribution of individual loss components. Applying \mathcal{L}_{MIM} alone degrades performance (e.g., 53.76% vs. 55.72% for

Table 3. **Performance Comparison with the reconstruction-based baseline.** (%) For fair comparison, we use the same model and datasets in [112]. LaVer outperforms ROSS on average.

Benchmark	CLIP-ViT-L/14@336			SigLIP-ViT-SO400M/14@384		
	Baseline	ROSS	LaVer	Baseline	ROSS	LaVer
MMB ^{EN}	66.15	↑1.41	↑4.55	70.96	↑0.63	↑1.78
SEED ^I	60.42	↑0.43	↑2.46	65.31	↓0.18	↑0.47
RWQA	53.07	↑0.69	↑0.09	57.39	↑1.22	↑3.26
MMM	36.78	↑0.70	↑4.44	37.56	↑1.00	↑0.66
OCRB	363	↑18	↑10	376	↑16	↑51
TVQA	38.05	↑2.10	↑4.24	52.56	↑1.26	↑3.19
CQA	27.04	↑3.13	↑4.32	34.40	↑1.87	↑0.72
AI2D	58.16	↑1.41	↑1.67	63.02	↑0.48	↑0.83
MMVP	58.67	↑12.71	↑10.53	68.00	↑8.60	↑5.00
Hallu	47.53	↑1.68	↑1.79	48.37	↑0.85	↑3.37
POPE	88.43	↑0.55	↑1.20	88.97	↑0.23	↑0.26
Average	48.59	↑2.25	↑2.91	53.36	↑1.45	↑1.78

SigLIP 2), empirically confirming the *visual feature inconsistency* phenomenon identified in Sec. 4.2, where visual information loss manifests as increased vision-token cosine similarity, diminishing visual structural information. While \mathcal{L}_{GA} preserves structure, it constrains discriminative learning. Conversely, \mathcal{L}_{CGA} achieves optimal performance by balancing structural fidelity with feature discrimination.

5.4. Discussion

Comparison with reconstruction-based baseline. We compare LaVer against ROSS [112], a reconstruction-based approach, under identical settings: Qwen2-7B-Instruct [119] with CLIP-ViT-L/14@336 [94] and SigLIP-ViT-SO400M/14@384 [126], trained on LLaVa-558K [67] and Cambrian-737K [102]. ROSS reconstructs low-level visual features, lacking semantic alignment with the language model’s embedding space. LaVer instead learns unified discriminative representations across modalities, directly mitigating modality imbalance. Table 3 shows LaVer achieves superior gains of 2.91% and 1.78% with CLIP and SigLIP respectively, outperforming ROSS’s 2.25% and 1.45%, with notable improvements on MMMU (+4.44% vs. +0.70%) and MMB^{EN} (+4.55% vs. +1.41%) using CLIP. Additional details are in the supplementary material.

Enhanced visual attention allocation. LaVer substantially increases visual attention allocation (Fig. 6), demonstrating improved visual information utilization and strengthened synergy between visual and textual modalities in the unified latent space. Additional quantitative and qualitative analyses are provided in the supplementary material.

6. Conclusion

This paper presents LaVer, a novel multimodal training framework that enables MLLMs to develop intrinsic visual representations within a unified high-level semantic space. A new regularizer is introduced to offer asymmetric guidances towards the visual feature deviation. With direct vi-

sual supervision from an online teacher, LaVer enhances visual information utilization and effectively addresses the modality imbalance prevalent in existing MLLMs. Our experiments demonstrate that explicit visual guidance during training substantially improves multimodal representations, yielding more robust and capable multimodal systems. We believe LaVer’s self-supervised paradigm offers a promising direction for advancing multimodal learning.

References

- [1] Hervé Abdi and Lynne J Williams. Principal component analysis. *Wiley Interdisciplinary Reviews: Computational Statistics*, 2010. 8
- [2] Jean-Baptiste Alayrac, Jeff Donahue, Pauline Luc, Antoine Miech, Iain Barr, Yana Hasson, Karel Lenc, Arthur Mensch, Katie Millican, Malcolm Reynolds, Roman Ring, Eliza Rutherford, Serkan Cabi, Tengda Han, Zhitao Gong, Sina Samangooei, Marianne Monteiro, Jacob Menick, Sebastian Borgeaud, Andrew Brock, Aida Nematzadeh, Sahand Sharifzadeh, Mikolaj Binkowski, Ricardo Barreira, Oriol Vinyals, Andrew Zisserman, and Karen Simonyan. Flamingo: a visual language model for few-shot learning. In *NeurIPS*, 2022. 1, 3
- [3] Xiang An, Yin Xie, Kaicheng Yang, Wenkang Zhang, Xiuwei Zhao, Zheng Cheng, Yirui Wang, Songcen Xu, Changrui Chen, Chunsheng Wu, Huajie Tan, Chunyuan Li, Jing Yang, Jie Yu, Xiyao Wang, Bin Qin, Yumeng Wang, Zizhen Yan, Ziyong Feng, Ziwei Liu, Bo Li, and Jiankang Deng. Llava-onevision-1.5: Fully open framework for democratized multimodal training. *arXiv*, 2509.23661, 2025. 1, 3, 4, 6, 5, 11
- [4] Stanislaw Antol, Aishwarya Agrawal, Jiasen Lu, Margaret Mitchell, Dhruv Batra, C. Lawrence Zitnick, and Devi Parikh. Vqa: Visual question answering. In *ICCV*, 2015. 1
- [5] Mahmoud Assran, Quentin Duval, Ishan Misra, Piotr Bojanowski, Pascal Vincent, Michael Rabbat, Yann LeCun, and Nicolas Ballas. Self-supervised learning from images with a joint-embedding predictive architecture. In *CVPR*, 2023. 3
- [6] Jinze Bai, Shuai Bai, Yunfei Chu, Zeyu Cui, Kai Dang, Xiaodong Deng, Yang Fan, Wenbin Ge, Yu Han, Fei Huang, Binyuan Hui, Luo Ji, Mei Li, Junyang Lin, Runji Lin, Dayiheng Liu, Gao Liu, Chengqiang Lu, Keming Lu, Jianxin Ma, Rui Men, Xingzhang Ren, Xuancheng Ren, Chuanqi Tan, Sinan Tan, Jianhong Tu, Peng Wang, Shijie Wang, Wei Wang, Shengguang Wu, Benfeng Xu, Jin Xu, An Yang, Hao Yang, Jian Yang, Shusheng Yang, Yang Yao, Bowen Yu, Hongyi Yuan, Zheng Yuan, Jianwei Zhang, Xingxuan Zhang, Yichang Zhang, Zhenru Zhang, Chang Zhou, Jingren Zhou, Xiaohuan Zhou, and Tianhang Zhu. Qwen technical report. *arXiv*, 2309.16609, 2023. 1, 3, 5
- [7] Jinze Bai, Shuai Bai, Shusheng Yang, Shijie Wang, Sinan Tan, Peng Wang, Junyang Lin, Chang Zhou, and Jingren Zhou. Qwen-vl: A versatile vision-language model for understanding, localization, text reading, and beyond. *arXiv*, 2308.12966, 2023. 1, 3
- [8] Shuai Bai, Keqin Chen, Xuejing Liu, Jialin Wang, Wenbin Ge, Sibao Song, Kai Dang, Peng Wang, Shijie Wang, Jun Tang, Humen Zhong, Yanzhi Zhu, Mingkun Yang, Zhaohai Li, Jianqiang Wan, Pengfei Wang, Wei Ding, Zheren Fu, Yiheng Xu, Jiabo Ye, Xi Zhang, Tianbao Xie, Zesen Cheng, Hang Zhang, Zhibo Yang, Haiyang Xu, and Junyang Lin. Qwen2.5-vl technical report. *arXiv*, 2502.13923, 2025. 1, 3, 5, 6, 7
- [9] Hangbo Bao, Li Dong, Songhao Piao, and Furu Wei. Beit: Bert pre-training of image transformers. In *ICLR*, 2022. 2, 3, 5
- [10] Adrien Bardes, Quentin Garrido, Jean Ponce, Xinlei Chen, Michael Rabbat, Yann LeCun, Mahmoud Assran, and Nicolas Ballas. Revisiting feature prediction for learning visual representations from video. *arXiv*, 2404.08471, 2024. 3
- [11] Tom Brown, Benjamin Mann, Nick Ryder, Melanie Subbiah, Jared D Kaplan, Prafulla Dhariwal, Arvind Neelakantan, Pranav Shyam, Girish Sastry, Amanda Askell, Sandhini Agarwal, Ariel Herbert-Voss, Gretchen Krueger, Tom Henighan, Rewon Child, Aditya Ramesh, Daniel Ziegler, Jeffrey Wu, Clemens Winter, Chris Hesse, Mark Chen, Eric Sigler, Mateusz Litwin, Scott Gray, Benjamin Chess, Jack Clark, Christopher Berner, Sam McCandlish, Alec Radford, Ilya Sutskever, and Dario Amodei. Language models are few-shot learners. In *NeurIPS*, 2020. 3
- [12] Tom B. Brown, Benjamin Mann, Nick Ryder, Melanie Subbiah, Jared Kaplan, Prafulla Dhariwal, Arvind Neelakantan, Pranav Shyam, Girish Sastry, Amanda Askell, Sandhini Agarwal, Ariel Herbert-Voss, Gretchen Krueger, Tom Henighan, Rewon Child, Aditya Ramesh, Daniel M. Ziegler, Jeffrey Wu, Clemens Winter, Christopher Hesse, Mark Chen, Eric Sigler, Mateusz Litwin, Scott Gray, Benjamin Chess, Jack Clark, Christopher Berner, Sam McCandlish, Alec Radford, Ilya Sutskever, and Dario Amodei. Language models are few-shot learners. In *NeurIPS*, 2020. 1
- [13] Holger Caesar, Jasper Uijlings, and Vittorio Ferrari. Cocomustuff: Thing and stuff classes in context. In *CVPR*, 2018. 7, 8
- [14] Holger Caesar, Varun Bankiti, Alex H. Lang, Sourabh Vora, Venice Erin Liong, Qiang Xu, Anush Krishnan, Yu Pan, Giancarlo Baldan, and Oscar Beijbom. nuscenes: A multimodal dataset for autonomous driving. In *CVPR*, 2020. 7, 8
- [15] Weitong Cai, Jiabo Huang, Shaogang Gong, Hailin Jin, and Yang Liu. Mllm as video narrator: Mitigating modality imbalance in video moment retrieval. *PR*, 2025. 1, 3
- [16] Yue Cao, Yangzhou Liu, Zhe Chen, Guangchen Shi, Wenhai Wang, Danhuai Zhao, and Tong Lu. Mmfuser: Multimodal multi-layer feature fuser for fine-grained vision-language understanding. *arXiv*, 2410.11829, 2024. 3
- [17] Mathilde Caron, Hugo Touvron, Ishan Misra, Hervé Jegou, Julien Mairal, Piotr Bojanowski, and Armand Joulin. Emerging properties in self-supervised vision transformers. In *ICCV*, 2021. 3, 8, 2, 10
- [18] Haonan Chen, Hong Liu, Yuping Luo, Liang Wang, Nan Yang, Furu Wei, and Zhicheng Dou. Moca: Modality-

aware continual pre-training makes better bidirectional multimodal embeddings. *arXiv*, 2506.23115, 2025. 5

- [19] Junyi Chen, Longteng Guo, Jia Sun, Shuai Shao, Zehuan Yuan, Liang Lin, and Dongyu Zhang. Eve: Efficient vision-language pre-training with masked prediction and modality-aware moe. In *AAAI*, 2024. 3
- [20] Lin Chen, Jinsong Li, Xiaoyi Dong, Pan Zhang, Yuhang Zang, Zehui Chen, Haodong Duan, Jiaqi Wang, Yu Qiao, Dahua Lin, and Feng Zhao. Are we on the right way for evaluating large vision-language models? In *NeurIPS*, 2024. 3, 6, 7
- [21] Liang Chen, Haozhe Zhao, Tianyu Liu, Shuai Bai, Junyang Lin, Chang Zhou, and Baobao Chang. An image is worth 1/2 tokens after layer 2: Plug-and-play inference acceleration for large vision-language models. In *ECCV*, 2024. 8
- [22] Meiqi Chen, Yixin Cao, Yan Zhang, and Chaochao Lu. Quantifying and mitigating unimodal biases in multimodal large language models: A causal perspective. In *EMNLP*, 2024. 1, 3
- [23] Yangyi Chen, Xingyao Wang, Hao Peng, and Heng Ji. A single transformer for scalable vision-language modeling. *TMLR*, 2024. 3, 6, 7
- [24] Jihoon Chung, Tyler Zhu, Max Gonzalez Saez-Diez, Juan Carlos Niebles, Honglu Zhou, and Olga Russakovsky. Unifying specialized visual encoders for video language models. In *ICML*, 2025. 3
- [25] X.AI Corp. Grok-1.5 vision preview: Connecting the digital and physical worlds with our first multimodal model, 2024. 6, 7
- [26] Wenliang Dai, Junnan Li, Dongxu Li, Anthony Meng Huat Tiong, Junqi Zhao, Weisheng Wang, Boyang Li, Pascale Fung, and Steven Hoi. Instructblip: towards general-purpose vision-language models with instruction tuning. In *NeurIPS*, 2023. 1, 3
- [27] DeepSeek-AI, Aixin Liu, Bei Feng, Bing Xue, Bingxuan Wang, Bochao Wu, Chengda Lu, Chenggang Zhao, Chengqi Deng, Chenyu Zhang, Chong Ruan, Damai Dai, Daya Guo, Dejian Yang, Deli Chen, Dongjie Ji, Erhang Li, Fangyun Lin, Fucong Dai, Fuli Luo, Guangbo Hao, Guanting Chen, Guowei Li, H. Zhang, Han Bao, Hanwei Xu, Haocheng Wang, Haowei Zhang, Honghui Ding, Huajian Xin, Huazuo Gao, Hui Li, Hui Qu, J. L. Cai, Jian Liang, Jianzhong Guo, Jiaqi Ni, Jiashi Li, Jiawei Wang, Jin Chen, Jingchang Chen, Jingyang Yuan, Junjie Qiu, Junlong Li, Junxiao Song, Kai Dong, Kai Hu, Kaige Gao, Kang Guan, Kexin Huang, Kuai Yu, Lean Wang, Lecong Zhang, Lei Xu, Leyi Xia, Liang Zhao, Litong Wang, Liyue Zhang, Meng Li, Miaojuan Wang, Mingchuan Zhang, Minghua Zhang, Minghui Tang, Mingming Li, Ning Tian, Panpan Huang, Peiyi Wang, Peng Zhang, Qiancheng Wang, Qihao Zhu, Qinyu Chen, Qiushi Du, R. J. Chen, R. L. Jin, Ruiqi Ge, Ruisong Zhang, Ruizhe Pan, Runji Wang, Runxin Xu, Ruoyu Zhang, Ruyi Chen, S. S. Li, Shanghao Lu, Shangyan Zhou, Shanhuang Chen, Shaoqing Wu, Shengfeng Ye, Shengfeng Ye, Shirong Ma, Shiyu Wang, Shuang Zhou, Shuiping Yu, Shunfeng Zhou, Shuting Pan, T. Wang, Tao Yun, Tian Pei, Tianyu Sun, W. L. Xiao, Wangding Zeng, Wanjia Zhao, Wei An, Wen Liu, Wenfeng Liang, Wenjun Gao, Wenqin Yu, Wentao Zhang, X. Q. Li, Xiangyue Jin, Xianzu Wang, Xiao Bi, Xiaodong Liu, Xiaohan Wang, Xiaojin Shen, Xiaokang Chen, Xiaokang Zhang, Xiaosha Chen, Xiaotao Nie, Xiaowen Sun, Xiaoxiang Wang, Xin Cheng, Xin Liu, Xin Xie, Xingchao Liu, Xingkai Yu, Xinnan Song, Xinxia Shan, Xinyi Zhou, Xinyu Yang, Xinyuan Li, Xuecheng Su, Xuheng Lin, Y. K. Li, Y. Q. Wang, Y. X. Wei, Y. X. Zhu, Yang Zhang, Yanhong Xu, Yanhong Xu, Yanping Huang, Yao Li, Yao Zhao, Yaofeng Sun, Yaohui Li, Yaohui Wang, Yi Yu, Yi Zheng, Yichao Zhang, Yifan Shi, Yiliang Xiong, Ying He, Ying Tang, Yishi Piao, Yisong Wang, Yixuan Tan, Yiyang Ma, Yiyuan Liu, Yongqiang Guo, Yu Wu, Yuan Ou, Yuchen Zhu, Yudian Wang, Yue Gong, Yuheng Zou, Yujia He, Yukun Zha, Yunfan Xiong, Yunxian Ma, Yuting Yan, Yuxiang Luo, Yuxiang You, Yuxuan Liu, Yuyang Zhou, Z. F. Wu, Z. Z. Ren, Zehui Ren, Zhangli Sha, Zhe Fu, Zhean Xu, Zhen Huang, Zhen Zhang, Zhenda Xie, Zhengyan Zhang, Zhewen Hao, Zhibin Gou, Zhicheng Ma, Zhigang Yan, Zhihong Shao, Zhipeng Xu, Zhiyu Wu, Zhongyu Zhang, Zhuoshu Li, Zihui Gu, Zijia Zhu, Zijun Liu, Zilin Li, Ziwei Xie, Ziyang Song, Ziyi Gao, and Zizheng Pan. Deepseek-v3 technical report. *arXiv*, 2412.19437, 2025. 3
- [28] Mostafa Dehghani, Basil Mustafa, Josip Djolonga, Jonathan Heek, Matthias Minderer, Mathilde Caron, Andreas Steiner, Joan Puigcerver, Robert Geirhos, Ibrahim Alabdulmohsin, Avital Oliver, Piotr Padlewski, Alexey Gritsenko, Mario Lučić, and Neil Houlsby. Patch n’ pack: Navit, a vision transformer for any aspect ratio and resolution. In *NeurIPS*, 2023. 3
- [29] Mostafa Dehghani, Basil Mustafa, Josip Djolonga, Jonathan Heek, Matthias Minderer, Mathilde Caron, Andreas Steiner, Joan Puigcerver, Robert Geirhos, Ibrahim M Alabdulmohsin, Avital Oliver, Piotr Padlewski, Alexey Gritsenko, Mario Lucic, and Neil Houlsby. Patch n’ pack: Navit, a vision transformer for any aspect ratio and resolution. In *NeurIPS*, 2023. 3
- [30] Haiwen Diao, Yufeng Cui, Xiaotong Li, Yueze Wang, Huchuan Lu, and Xinlong Wang. Unveiling encoder-free vision-language models. In *NeurIPS*, 2024. 3, 7
- [31] Shizhe Diao, Wangchunshu Zhou, Xinsong Zhang, and Jiawei Wang. Write and paint: Generative vision-language models are unified modal learners. In *ICML*, 2023. 3
- [32] Carl Doersch, Abhinav Gupta, and Alexei A. Efros. Unsupervised visual representation learning by context prediction. In *ICCV*, 2015. 3
- [33] Carl Doersch, Abhinav Gupta, and Alexei A. Efros. Unsupervised visual representation learning by context prediction. In *ICCV*, 2016. 3
- [34] Alexey Dosovitskiy, Lucas Beyer, Alexander Kolesnikov, Dirk Weissenborn, Xiaohua Zhai, Thomas Unterthiner, Mostafa Dehghani, Matthias Minderer, Georg Heigold, Sylvain Gelly, Jakob Uszkoreit, and Neil Houlsby. An image is worth 16x16 words: Transformers for image recognition at scale. In *ICLR*, 2021. 5
- [35] Haodong Duan, Junming Yang, Yuxuan Qiao, Xinyu Fang, Lin Chen, Yuan Liu, Xiaoyi Dong, Yuhang Zang, Pan

- Zhang, Jiaqi Wang, Dahua Lin, and Kai Chen. Vlmevalkit: An open-source toolkit for evaluating large multi-modality models. In *ACM MM*, 2024. 6, 7
- [36] Patrick Esser, Robin Rombach, and Björn Ommer. Taming transformers for high-resolution image synthesis. In *CVPR*, 2021. 3
- [37] David Fan, Shengbang Tong, Jiachen Zhu, Koustuv Sinha, Zhuang Liu, Xinlei Chen, Michael Rabbat, Nicolas Ballas, Yann LeCun, Amir Bar, and Saining Xie. Scaling language-free visual representation learning. In *ICCV*, 2025. 5
- [38] Enrico Fini, Mustafa Shukor, Xiujun Li, Philipp Dufter, Michal Klein, David Haldimann, Sai Aitharaju, Victor Costa, Louis Béthune, Zhe Gan, Alexander Toshev, Marcin Eichner, Moin Nabi, Yinfei Yang, Joshua Susskind, and Alaa El-Nouby. Multimodal autoregressive pre-training of large vision encoders. In *CVPR*, 2025. 3, 6, 7
- [39] Chaoyou Fu, Peixian Chen, Yunhang Shen, Yulei Qin, Mengdan Zhang, Xu Lin, Jinrui Yang, Xiawu Zheng, Ke Li, Xing Sun, Yunsheng Wu, Rongrong Ji, Caifeng Shan, and Ran He. Mme: A comprehensive evaluation benchmark for multimodal large language models. In *NeurIPS*, 2025. 1, 6, 7, 9
- [40] Xinyang Geng, Hao Liu, Lisa Lee, Dale Schuurmans, Sergey Levine, and Pieter Abbeel. Multimodal masked autoencoders learn transferable representations. In *ICML*, 2022. 3
- [41] Spyros Gidaris, Andrei Bursuc, Nikos Komodakis, Patrick Pérez, and Matthieu Cord. Boosting few-shot visual learning with self-supervision. In *ICCV*, 2019. 3
- [42] Spyros Gidaris, Andrei Bursuc, Oriane Simeoni, Antonin Vobecky, Nikos Komodakis, Matthieu Cord, and Patrick Pérez. Moca: Self-supervised representation learning by predicting masked online codebook assignments. *TMLR*, 2024. 2
- [43] Aaron Grattafiori, Abhimanyu Dubey, Abhinav Jauhri, Abhinav Pandey, Abhishek Kadian, Ahmad Al-Dahle, Aiesha Letman, Akhil Mathur, Alan Schelten, Alex Vaughan, Amy Yang, Angela Fan, Anirudh Goyal, Anthony Hartshorn, Aobo Yang, Archi Mitra, Archie Sravankumar, Artem Korenev, Arthur Hinsvark, Arun Rao, Aston Zhang, Aurelien Rodriguez, Austen Gregerson, Ava Spataru, Baptiste Roziere, Bethany Biron, Binh Tang, Bobbie Chern, Charlotte Caucheteux, Chaya Nayak, Chloe Bi, Chris Marra, Chris McConnell, Christian Keller, Christophe Touret, Chunyang Wu, Corinne Wong, Cristian Canton Ferrer, Cyrus Nikolaidis, Damien Allonsius, Daniel Song, Danielle Pintz, Danny Livshits, Danny Wyatt, David Esiobu, Dhruv Choudhary, Dhruv Mahajan, Diego Garcia-Olano, Diego Perino, Dieuwke Hupkes, Egor Lakomkin, Ehab Al-Badawy, Elina Lobanova, Emily Dinan, Eric Michael Smith, Filip Radenovic, Francisco Guzmán, Frank Zhang, Gabriel Synnaeve, Gabrielle Lee, Georgia Lewis Anderson, Govind Thattai, Graeme Nail, Gregoire Mialon, Guan Pang, Guillem Cucurell, Hailey Nguyen, Hannah Korevaar, Hu Xu, Hugo Touvron, Iliyan Zarov, Imanol Arrieta Ibarra, Isabel Kloumann, Ishan Misra, Ivan Evtimov, Jack Zhang, Jade Copet, Jaewon Lee, Jan Geffert, Jana Vranes, Jason Park, Jay Mahadeokar, Jeet Shah, Jelmer van der Linde, Jennifer Billock, Jenny Hong, Jenya Lee, Jeremy Fu, Jianfeng Chi, Jianyu Huang, Jiawen Liu, Jie Wang, Jiecao Yu, Joanna Bitton, Joe Spisak, Jongsoo Park, Joseph Rocca, Joshua Johnstun, Joshua Saxe, Junteng Jia, Kalyan Vasuden Alwala, Karthik Prasad, Kartikeya Upasani, Kate Plawiak, Ke Li, Kenneth Heafield, Kevin Stone, Khalid El-Arini, Krithika Iyer, Kshitiz Malik, Kuenley Chiu, Kunal Bhalla, Kushal Lakhotia, Lauren Rantala-Yearly, Laurens van der Maaten, Lawrence Chen, Liang Tan, Liz Jenkins, Louis Martin, Lovish Madaan, Lubo Malo, Lukas Blecher, Lukas Landzaat, Luke de Oliveira, Madeline Muzzi, Mahesh Pasupuleti, Mannat Singh, Manohar Paluri, Marcin Kardas, Maria Tsimploukelli, Mathew Oldham, Mathieu Rita, Maya Pavlova, Melanie Kambadur, Mike Lewis, Min Si, Mitesh Kumar Singh, Mona Hassan, Naman Goyal, Narjes Torabi, Nikolay Bashlykov, Nikolay Bogoychev, Niladri Chatterji, Ning Zhang, Olivier Duchenne, Onur Çelebi, Patrick Alrassy, Pengchuan Zhang, Pengwei Li, Petar Vasic, Peter Weng, Prajjwal Bhargava, Pratik Dubal, Praveen Krishnan, Punit Singh Koura, Puxin Xu, Qing He, Qingxiao Dong, Ragavan Srinivasan, Raj Ganapathy, Ramon Calderer, Ricardo Silveira Cabral, Robert Stojnic, Roberta Raileanu, Rohan Maheswari, Rohit Girdhar, Rohit Patel, Romain Sauvestre, Ronnie Polidoro, Roshan Sumbaly, Ross Taylor, Ruan Silva, Rui Hou, Rui Wang, Saghar Hosseini, Sahana Chennabasappa, Sanjay Singh, Sean Bell, Seohyun Sonia Kim, Sergey Edunov, Shaoqiang Nie, Sharan Narang, Sharath Raparthy, Sheng Shen, Shengye Wan, Shruti Bhosale, Shun Zhang, Simon Vandenhende, Soumya Batra, Spencer Whitman, Sten Sootla, Stephane Collot, Suchin Gururangan, Sydney Borodinsky, Tamar Herman, Tara Fowler, Tarek Sheasha, Thomas Georgiou, Thomas Scialom, Tobias Speckbacher, Todor Mihaylov, Tong Xiao, Ujjwal Karn, Vedanuj Goswami, Vibhor Gupta, Vignesh Ramanathan, Viktor Kerkez, Vincent Gonguet, Virginie Do, Vish Voleti, Vitor Albiero, Vladan Petrovic, Weiwei Chu, Wenhan Xiong, Wenyin Fu, Whitney Meers, Xavier Martinet, Xiaodong Wang, Xiaofang Wang, Xiaoqing Ellen Tan, Xide Xia, Xinfeng Xie, Xuchao Jia, Xuewei Wang, Yaelle Goldschlag, Yashesh Gaur, Yasmine Babaei, Yi Wen, Yiwen Song, Yuchen Zhang, Yue Li, Yuning Mao, Zacharie Delpierre Coudert, Zheng Yan, Zhengxing Chen, Zoe Papakipos, Aaditya Singh, Aayushi Srivastava, Abha Jain, Adam Kelsey, Adam Shajnfeld, Adithya Gangidi, Adolfo Victoria, Ahuva Goldstand, Ajay Menon, Ajay Sharma, Alex Boesenberg, Alexei Baevski, Allie Feinstein, Amanda Kallet, Amit Sangani, Amos Teo, Anam Yunus, Andrei Lupu, Andres Alvarado, Andrew Caples, Andrew Gu, Andrew Ho, Andrew Poulton, Andrew Ryan, Ankit Ramchandani, Annie Dong, Annie Franco, Anuj Goyal, Aparajita Saraf, Arkabandhu Chowdhury, Ashley Gabriel, Ashwin Barambe, Assaf Eisenman, Azadeh Yazdan, Beau James, Ben Maurer, Benjamin Leonhardi, Bernie Huang, Beth Loyd, Beto De Paola, Bhargavi Paranjape, Bing Liu, Bo Wu, Boyu Ni, Braden Hancock, Bram Wasti, Brandon Spence, Brani Stojkovic, Brian Gamido, Britt Montalvo, Carl Parker, Carly Burton, Catalina Mejia, Ce Liu, Changhan Wang, Changkyu Kim, Chao Zhou, Chester Hu, Ching-

Hsiang Chu, Chris Cai, Chris Tindal, Christoph Feichtenhof, Cynthia Gao, Damon Civin, Dana Beaty, Daniel Kreymer, Daniel Li, David Adkins, David Xu, Davide Testuggine, Delia David, Devi Parikh, Diana Liskovich, Didem Foss, Dingkan Wang, Duc Le, Dustin Holland, Edward Dowling, Eissa Jamil, Elaine Montgomery, Eleonora Presani, Emily Hahn, Emily Wood, Eric-Tuan Le, Erik Brinkman, Esteban Arcaute, Evan Dunbar, Evan Smothers, Fei Sun, Felix Kreuk, Feng Tian, Filippus Kokkinos, Firat Ozgenel, Francesco Caggioni, Frank Kanayet, Frank Seide, Gabriela Medina Florez, Gabriella Schwarz, Gada Badeer, Georgia Swee, Gil Halpern, Grant Herman, Grigory Sizov, Guangyi, Zhang, Guna Lakshminarayanan, Hakan Inan, Hamid Shojanazeri, Han Zou, Hannah Wang, Hanwen Zha, Haroun Habeeb, Harrison Rudolph, Helen Suk, Henry Aspegren, Hunter Goldman, Hongyuan Zhan, Ibrahim Damlaj, Igor Molybog, Igor Tufanov, Ilias Leontiadis, Irina-Elena Veliche, Itai Gat, Jake Weissman, James Geboski, James Kohli, Janice Lam, Japhet Asher, Jean-Baptiste Gaya, Jeff Marcus, Jeff Tang, Jennifer Chan, Jenny Zhen, Jeremy Reizenstein, Jeremy Teboul, Jessica Zhong, Jian Jin, Jingyi Yang, Joe Cummings, Jon Carvill, Jon Shepard, Jonathan McPhie, Jonathan Torres, Josh Ginsburg, Junjie Wang, Kai Wu, Kam Hou U, Karan Saxena, Kartikay Khandelwal, Katayoun Zand, Kathy Matosich, Kaushik Veeraraghavan, Kelly Michelena, Keqian Li, Kiran Jagadeesh, Kun Huang, Kunal Chawla, Kyle Huang, Lailin Chen, Lakshya Garg, Lavender A, Leandro Silva, Lee Bell, Lei Zhang, Liangpeng Guo, Licheng Yu, Liron Moshkovich, Luca Wehrstedt, Madian Khabza, Manav Avalani, Manish Bhatt, Martynas Mankus, Matan Hasson, Matthew Lennie, Matthias Reso, Maxim Groshev, Maxim Naumov, Maya Lathi, Meghan Keneally, Miao Liu, Michael L. Seltzer, Michal Valko, Michelle Restrepo, Mihir Patel, Mik Vyatskov, Mikayel Samvelyan, Mike Clark, Mike Macey, Mike Wang, Miquel Jubert Hermoso, Mo Metanat, Mohammad Rastegari, Munish Bansal, Nandhini Santhanam, Natascha Parks, Natasha White, Navyata Bawa, Nayan Singhal, Nick Egebo, Nicolas Usunier, Nikhil Mehta, Nikolay Pavlovich Laptev, Ning Dong, Norman Cheng, Oleg Chernoguz, Olivia Hart, Omkar Salpekar, Ozlem Kalinli, Parkin Kent, Parth Parekh, Paul Saab, Pavan Balaji, Pedro Rittner, Philip Bontrager, Pierre Roux, Piotr Dollar, Polina Zvyagina, Prashant Ratanchandani, Pritish Yuvraj, Qian Liang, Rachad Alao, Rachel Rodriguez, Rafi Ayub, Raghotham Murthy, Raghu Nayani, Rahul Mitra, Rangaprabhu Parthasarathy, Raymond Li, Rebekkah Hogan, Robin Battey, Rocky Wang, Russ Howes, Ruty Rinott, Sachin Mehta, Sachin Siby, Sai Jayesh Bondu, Samyak Datta, Sara Chugh, Sara Hunt, Sargun Dhillon, Sasha Sidorov, Satadru Pan, Saurabh Mahajan, Saurabh Verma, Seiji Yamamoto, Sharadh Ramaswamy, Shaun Lindsay, Shaun Lindsay, Sheng Feng, Shenghao Lin, Shengxin Cindy Zha, Shishir Patil, Shiva Shankar, Shuqiang Zhang, Shuqiang Zhang, Sinong Wang, Sneha Agarwal, Soji Sajuyigbe, Soumith Chintala, Stephanie Max, Stephen Chen, Steve Kehoe, Steve Satterfield, Sudarshan Govindaprasad, Sumit Gupta, Summer Deng, Sung-

min Cho, Sunny Virk, Suraj Subramanian, Sy Choudhury, Sydney Goldman, Tal Remez, Tamar Glaser, Tamara Best, Thilo Koehler, Thomas Robinson, Tianhe Li, Tianjun Zhang, Tim Matthews, Timothy Chou, Tzook Shaked, Varun Vontimitta, Victoria Ajayi, Victoria Montanez, Vijai Mohan, Vinay Satish Kumar, Vishal Mangla, Vlad Ionescu, Vlad Poenaru, Vlad Tiberiu Mihailescu, Vladimir Ivanov, Wei Li, Wenchen Wang, Wenwen Jiang, Wes Bouaziz, Will Constable, Xiaocheng Tang, Xiaojian Wu, Xiaolan Wang, Xilun Wu, Xinbo Gao, Yaniv Kleinman, Yanjun Chen, Ye Hu, Ye Jia, Ye Qi, Yenda Li, Yilin Zhang, Ying Zhang, Yossi Adi, Youngjin Nam, Yu, Wang, Yu Zhao, Yuchen Hao, Yundi Qian, Yunlu Li, Yuzi He, Zach Rait, Zachary DeVito, Zef Rosnbrick, Zhaoduo Wen, Zhenyu Yang, Zhiwei Zhao, and Zhiyu Ma. The llama 3 herd of models. *Meta*, 2024. 1, 3

- [44] Tianrui Guan, Fuxiao Liu, Xiyang Wu, Ruiqi Xian, Zongxia Li, Xiaoyu Liu, Xijun Wang, Lichang Chen, Furong Huang, Yaser Yacoob, Dinesh Manocha, and Tianyi Zhou. Hallusionbench: An advanced diagnostic suite for entangled language hallucination and visual illusion in large vision-language models. In *CVPR*, 2024. 1, 6, 7
- [45] Vipul Gupta, Zhuowan Li, Adam Kortylewski, Chenyu Zhang, Yingwei Li, and Alan Yuille. Swapmix: Diagnosing and regularizing the over-reliance on visual context in visual question answering. In *CVPR*, 2022. 3
- [46] Kaiming He, Xinlei Chen, Saining Xie, Yanghao Li, Piotr Dollár, and Ross Girshick. Masked autoencoders are scalable vision learners. In *CVPR*, 2022. 2, 3, 5
- [47] Dan Hendrycks, Collin Burns, Steven Basart, Andy Zou, Mantas Mazeika, Dawn Song, and Jacob Steinhardt. Measuring massive multitask language understanding. In *ICLR*, 2021. 11
- [48] Byeongho Heo, Song Park, Dongyoon Han, and Sangdoo Yun. Rotary position embedding for vision transformer. In *ECCV*, 2024. 5
- [49] Drew A. Hudson and Christopher D. Manning. Gqa: A new dataset for real-world visual reasoning and compositional question answering. In *CVPR*, 2019. 6, 7
- [50] Minyoung Huh, Brian Cheung, Tongzhou Wang, and Phillip Isola. The platonic representation hypothesis. *arXiv*, 2405.07987, 2024. 1
- [51] Hongrui Jia, Chaoya Jiang, Haiyang Xu, Wei Ye, Mengfan Dong, Ming Yan, Ji Zhang, Fei Huang, and Shikun Zhang. Sympo: Boosting in-context learning of large multimodal models with symbol demonstration direct preference optimization. In *CVPR*, 2024. 1
- [52] Zhangqi Jiang, Junkai Chen, Beier Zhu, Tingjin Luo, Yankun Shen, and Xu Yang. Devils in middle layers of large vision-language models: Interpreting, detecting and mitigating object hallucinations via attention lens. In *CVPR*, 2025. 2
- [53] Aniruddha Kembhavi, Michael Salvato, Eric Kolve, Minjoon Seo, Hannaneh Hajishirzi, and Ali Farhadi. A diagram is worth a dozen images. In *ECCV*, 2016. 6, 7
- [54] Simon Kornblith, Mohammad Norouzi, Honglak Lee, and Geoffrey Hinton. Similarity of neural network representations revisited. In *ICML*, 2019. 1

- [55] Xin Lai, Zhuotao Tian, Yukang Chen, Yanwei Li, Yuhui Yuan, Shu Liu, and Jiaya Jia. Lisa: Reasoning segmentation via large language model. In *CVPR*, 2024. 3, 7
- [56] Weixian Lei, Jiacong Wang, Haochen Wang, Xiangtai Li, Jun Hao Liew, Jiashi Feng, and Zilong Huang. The scalability of simplicity: Empirical analysis of vision-language learning with a single transformer. In *ICCV*, 2025. 3, 5, 6, 7, 8
- [57] Sicong Leng, Yun Xing, Zesen Cheng, Yang Zhou, Hang Zhang, Xin Li, Deli Zhao, Shijian Lu, Chunyan Miao, and Lidong Bing. The curse of multi-modalities: Evaluating hallucinations of large multimodal models across language, visual, and audio. *arXiv*, 2410.12787, 2024. 1
- [58] Sicong Leng, Hang Zhang, Guanzheng Chen, Xin Li, Shijian Lu, Chunyan Miao, and Lidong Bing. Mitigating object hallucinations in large vision-language models through visual contrastive decoding. In *CVPR*, 2024. 1
- [59] Bohao Li, Rui Wang, Guangzhi Wang, Yuying Ge, Yixiao Ge, and Ying Shan. Seed-bench: Benchmarking multimodal llms with generative comprehension. In *CVPR*, 2024. 6, 7
- [60] Bo Li, Yuanhan Zhang, Dong Guo, Renrui Zhang, Feng Li, Hao Zhang, Kaichen Zhang, Peiyuan Zhang, Yanwei Li, Ziwei Liu, and Chunyuan Li. LLaVA-onevision: Easy visual task transfer. *TMLR*, 2025. 1, 3, 6
- [61] Chengzu Li, Wenshan Wu, Huanyu Zhang, Yan Xia, Shaoguang Mao, Li Dong, Ivan Vulić, and Furu Wei. Imagine while reasoning in space: Multimodal visualization-of-thought. *arXiv*, 2501.07542, 2025. 1
- [62] Feng Li, Renrui Zhang, Hao Zhang, Yuanhan Zhang, Bo Li, Wei Li, Zejun MA, and Chunyuan Li. LLaVA-neXT-interleave: Tackling multi-image, video, and 3d in large multimodal models. In *ICLR*, 2025. 3
- [63] Yifan Li, Yifan Du, Kun Zhou, Jinpeng Wang, Xin Zhao, and Ji-Rong Wen. Evaluating object hallucination in large vision-language models. In *EMNLP*, 2023. 6, 7
- [64] Zichao Li, Xueru Wen, Jie Lou, Yuqiu Ji, Yaojie Lu, Xi-anpei Han, Debing Zhang, and Le Sun. The devil is in the details: Tackling unimodal spurious correlations for generalizable multimodal reward models. In *ICML*, 2025. 3
- [65] Junyan Lin, Haoran Chen, Yue Fan, Yingqi Fan, Xin Jin, Hui Su, Jinlan Fu, and Xiaoyu Shen. Multi-layer visual feature fusion in multimodal llms: Methods, analysis, and best practices. In *CVPR*, 2025. 3
- [66] Haotian Liu, Chunyuan Li, Yuheng Li, and Yong Jae Lee. Improved baselines with visual instruction tuning. *arXiv*, 2310.03744, 2023. 1, 3, 7, 8
- [67] Haotian Liu, Chunyuan Li, Qingyang Wu, and Yong Jae Lee. Visual instruction tuning. In *NeurIPS*, 2023. 3, 6, 8
- [68] Haotian Liu, Chunyuan Li, Yuheng Li, Bo Li, Yuanhan Zhang, Sheng Shen, and Yong Jae Lee. Llava-next: Improved reasoning, ocr, and world knowledge. *arXiv*, 2310.03744, 2024. 1, 3
- [69] Xiaoyuan Liu, Wenxuan Wang, Youliang Yuan, Jen tse Huang, Qiuzhi Liu, Pinjia He, and Zhaopeng Tu. Insight over sight: Exploring the vision-knowledge conflicts in multimodal llms. In *ACL*, 2025. 1, 3
- [70] Yuan Liu, Haodong Duan, Yuanhan Zhang, Bo Li, Songyang Zhang, Wangbo Zhao, Yike Yuan, Jiaqi Wang, Conghui He, Ziwei Liu, Kai Chen, and Dahua Lin. Mmbench: Is your multi-modal model an all-around player? In *ECCV*, 2024. 6, 7
- [71] Yuliang Liu, Zhang Li, Mingxin Huang, Biao Yang, Wenwen Yu, Chunyuan Li, Xu-Cheng Yin, Cheng-Lin Liu, Lianwen Jin, and Xiang Bai. Ocrbench: on the hidden mystery of ocr in large multimodal models. *Science China Information Sciences*, 2024. 1, 2, 6, 7, 9
- [72] Ze Liu, Yutong Lin, Yue Cao, Han Hu, Yixuan Wei, Zheng Zhang, Stephen Lin, and Baining Guo. Swin transformer: Hierarchical vision transformer using shifted windows. In *ICCV*, 2021. 5
- [73] Zujing Liu, Junwen Pan, Qi She, Yuan Gao, and Guisong Xia. On the faithfulness of visual thinking: Measurement and enhancement. *arXiv*, 2510.23482, 2025. 1, 3
- [74] Haoyu Lu, Wen Liu, Bo Zhang, Bingxuan Wang, Kai Dong, Bo Liu, Jingxiang Sun, Tongzheng Ren, Zhuoshu Li, Hao Yang, Yaofeng Sun, Chengqi Deng, Hanwei Xu, Zhenda Xie, and Chong Ruan. Deepseek-vl: Towards real-world vision-language understanding. *arXiv*, 2403.05525, 2024. 3
- [75] Pan Lu, Swaroop Mishra, Tony Xia, Liang Qiu, Kai-Wei Chang, Song-Chun Zhu, Oyvind Tafjord, Peter Clark, and Ashwin Kalyan. Learn to explain: Multimodal reasoning via thought chains for science question answering. In *NeurIPS*, 2022. 6, 7
- [76] Pan Lu, Hritik Bansal, Tony Xia, Jiacheng Liu, Chunyuan Li, Hannaneh Hajishirzi, Hao Cheng, Kai-Wei Chang, Michel Galley, and Jianfeng Gao. Mathvista: Evaluating mathematical reasoning of foundation models in visual contexts. In *ICLR*, 2024. 6, 7, 9
- [77] Yuanhuiyi Lyu, Xu Zheng, Jiazhou Zhou, and Lin Wang. Unibind: Llm-augmented unified and balanced representation space to bind them all. In *CVPR*, 2024. 2
- [78] Ahmed Masry, Do Xuan Long, Jia Qing Tan, Shafiq Joty, and Enamul Hoque. ChartQA: A benchmark for question answering about charts with visual and logical reasoning. In *ACL*, 2022. 1, 2, 6, 7, 9, 11
- [79] Brandon McKinzie, Zhe Gan, Jean-Philippe Fauconnier, Sam Dodge, Bowen Zhang, Philipp Dufter, Dhruvi Shah, Xianzhi Du, Futang Peng, Floris Weers, Anton Belyi, Haotian Zhang, Karanjeet Singh, Doug Kang, Ankur Jain, Hongyu Hè, Max Schwarzer, Tom Gunter, Xiang Kong, Aonan Zhang, Jianyu Wang, Chong Wang, Nan Du, Tao Lei, Sam Wiseman, Guoli Yin, Mark Lee, Zirui Wang, Ruoming Pang, Peter Gräsch, Alexander Toshev, and Yin-fei Yang. Mm1: Methods, analysis & insights from multimodal llm pre-training. *arXiv*, 2403.09611, 2024. 3
- [80] Ishan Misra and Laurens van der Maaten. Self-supervised learning of pretext-invariant representations. In *CVPR*, 2020. 3
- [81] Marco Mistretta, Alberto Baldrati, Lorenzo Agnolucci, Marco Bertini, and Andrew D. Bagdanov. Cross the gap: Exposing the intra-modal misalignment in CLIP via modality inversion. In *ICLR*, 2025. 3

- [82] JeongYeon Nam, Jinbae Im, Wonjae Kim, and Taeho Kil. Extract free dense misalignment from clip. In *AAAI*, 2025. 3
- [83] Gerhard Neuhold, Tobias Ollmann, Samuel Rota Bulò, and Peter Kotschieder. The mapillary vistas dataset for semantic understanding of street scenes. In *ICCV*, 2017. 7, 8
- [84] Yulei Niu, Kaihua Tang, Hanwang Zhang, Zhiwu Lu, Xian-Sheng Hua, and Ji-Rong Wen. Counterfactual vqa: A cause-effect look at language bias. In *CVPR*, 2021. 3
- [85] Mehdi Noroozi and Paolo Favaro. Unsupervised learning of visual representations by solving jigsaw puzzles. In *ECCV*, 2016. 3
- [86] OpenAI, Josh Achiam, Steven Adler, Sandhini Agarwal, Lama Ahmad, Ilge Akkaya, Florencia Leoni Aleman, Diogo Almeida, Janko Altschmidt, Sam Altman, Shyamal Anadkat, Red Avila, Igor Babuschkin, Suchir Balaji, Valerie Balcom, Paul Baltescu, Haiming Bao, Mohammad Bavarian, Jeff Belgum, Irwan Bello, Jake Berdine, Gabriel Bernadett-Shapiro, Christopher Berner, Lenny Bogdonoff, Oleg Boiko, Madelaine Boyd, Anna-Luisa Brakman, Greg Brockman, Tim Brooks, Miles Brundage, Kevin Button, Trevor Cai, Rosie Campbell, Andrew Cann, Brittany Carey, Chelsea Carlson, Rory Carmichael, Brooke Chan, Che Chang, Fotis Chantzis, Derek Chen, Sully Chen, Ruby Chen, Jason Chen, Mark Chen, Ben Chess, Chester Cho, Casey Chu, Hyung Won Chung, Dave Cummings, Jeremiah Currier, Yunxing Dai, Cory Decareaux, Thomas Degry, Noah Deutsch, Damien Deville, Arka Dhar, David Dohan, Steve Dowling, Sheila Dunning, Adrien Ecoffet, Atty Eleti, Tyna Eloundou, David Farhi, Liam Fedus, Niko Felix, Simón Posada Fishman, Juston Forte, Isabella Fulford, Leo Gao, Elie Georges, Christian Gibson, Vik Goel, Tarun Gogineni, Gabriel Goh, Rapha Gontijo-Lopes, Jonathan Gordon, Morgan Grafstein, Scott Gray, Ryan Greene, Joshua Gross, Shixiang Shane Gu, Yufei Guo, Chris Hallacy, Jesse Han, Jeff Harris, Yuchen He, Mike Heaton, Johannes Heidecke, Chris Hesse, Alan Hickey, Wade Hickey, Peter Hoeschele, Brandon Houghton, Kenny Hsu, Shengli Hu, Xin Hu, Joost Huizinga, Shantanu Jain, Shawn Jain, Joanne Jang, Angela Jiang, Roger Jiang, Haozhun Jin, Denny Jin, Shino Jomoto, Billie Jonn, Heewoo Jun, Tomer Kaftan, Łukasz Kaiser, Ali Kamali, Ingmar Kanitscheider, Nitish Shirish Keskar, Tabarak Khan, Logan Kilpatrick, Jong Wook Kim, Christina Kim, Yongjik Kim, Jan Hendrik Kirchner, Jamie Kiros, Matt Knight, Daniel Kokotajlo, Łukasz Kondraciuk, Andrew Kondrich, Aris Konstantinidis, Kyle Kosic, Gretchen Krueger, Vishal Kuo, Michael Lampe, Ikai Lan, Teddy Lee, Jan Leike, Jade Leung, Daniel Levy, Chak Ming Li, Rachel Lim, Molly Lin, Stephanie Lin, Mateusz Litwin, Theresa Lopez, Ryan Lowe, Patricia Lue, Anna Makanju, Kim Malfacini, Sam Manning, Todor Markov, Yaniv Markovski, Bianca Martin, Katie Mayer, Andrew Mayne, Bob McGrew, Scott Mayer McKinney, Christine McLeavey, Paul McMillan, Jake McNeil, David Medina, Aalok Mehta, Jacob Menick, Luke Metz, Andrey Mishchenko, Pamela Mishkin, Vinnie Monaco, Evan Morikawa, Daniel Mossing, Tong Mu, Mira Murati, Oleg Murk, David Mély, Ashvin Nair, Reiichiro Nakano, Rajeev Nayak, Arvind Neelakantan, Richard Ngo, Hyeonwoo Noh, Long Ouyang, Cullen O’Keefe, Jakub Pachocki, Alex Paino, Joe Palermo, Ashley Pantuliano, Giambattista Parascandolo, Joel Parish, Emy Parparita, Alex Passos, Mikhail Pavlov, Andrew Peng, Adam Perelman, Filipe de Avila Belbute Peres, Michael Petrov, Henrique Ponde de Oliveira Pinto, Michael, Pokorny, Michelle Pokrass, Vitchyr H. Pong, Tolly Powell, Alethea Power, Boris Power, Elizabeth Proehl, Raul Puri, Alec Radford, Jack Rae, Aditya Ramesh, Cameron Raymond, Francis Real, Kendra Rimbach, Carl Ross, Bob Rotsted, Henri Roussez, Nick Ryder, Mario Saltarelli, Ted Sanders, Shibani Santurkar, Girish Sastry, Heather Schmidt, David Schnurr, John Schulman, Daniel Selsam, Kyla Sheppard, Toki Sherbakov, Jessica Shieh, Sarah Shoker, Pranav Shyam, Szymon Sidor, Eric Sigler, Maddie Simens, Jordan Sitkin, Katarina Slama, Ian Sohl, Benjamin Sokolowsky, Yang Song, Natalie Staudacher, Felipe Petroski Such, Natalie Summers, Ilya Sutskever, Jie Tang, Nikolas Tezak, Madeleine B. Thompson, Phil Tillet, Amin Tootoonchian, Elizabeth Tseng, Preston Tuggle, Nick Turley, Jerry Tworek, Juan Felipe Cerón Uribe, Andrea Vallone, Arun Vijayvergiya, Chelsea Voss, Carroll Wainwright, Justin Jay Wang, Alvin Wang, Ben Wang, Jonathan Ward, Jason Wei, CJ Weinmann, Akila Welihinda, Peter Welinder, Jiayi Weng, Lilian Weng, Matt Wiethoff, Dave Willner, Clemens Winter, Samuel Wolrich, Hannah Wong, Lauren Workman, Sherwin Wu, Jeff Wu, Michael Wu, Kai Xiao, Tao Xu, Sarah Yoo, Kevin Yu, Qiming Yuan, Wojciech Zaremba, Rowan Zellers, Chong Zhang, Marvin Zhang, Shengjia Zhao, Tianhao Zheng, Juntang Zhuang, William Zhuk, and Barret Zoph. Gpt-4 technical report. *OpenAI*, 2024. 1, 3
- [87] Maxime Oquab, Timothée Darcet, Théo Moutakanni, Huy V. Vo, Marc Szafraniec, Vasil Khalidov, Pierre Fernandez, Daniel HAZIZA, Francisco Massa, Alaaeldin El-Nouby, Mido Assran, Nicolas Ballas, Wojciech Galuba, Russell Howes, Po-Yao Huang, Shang-Wen Li, Ishan Misra, Michael Rabbat, Vasu Sharma, Gabriel Synnaeve, Hu Xu, Herve Jegou, Julien Mairal, Patrick Labatut, Armand Joulin, and Piotr Bojanowski. DINOv2: Learning robust visual features without supervision. *TMLR*, 2024. 1, 3, 5, 6, 8, 2, 10, 11
- [88] Jean Park, Kuk Jin Jang, Basam Alasaly, Sriharsha Mopidevi, Andrew Zolensky, Eric Eaton, Insup Lee, and Kevin Johnson. Assessing modality bias in video question answering benchmarks with multimodal large language models. In *AAAI*, 2025. 1, 3
- [89] Renjie Pi, Tianyang Han, Wei Xiong, Jipeng Zhang, Runtao Liu, Rui Pan, and Tong Zhang. Strengthening multimodal large language model with bootstrapped preference optimization. In *ECCV*, 2024. 3
- [90] Jianing Qi, Jiawei Liu, Hao Tang, and Zhigang Zhu. Beyond semantics: Rediscovering spatial awareness in vision-language models. *arXiv*, 2503.17349, 2025. 1
- [91] Qwen, :, An Yang, Baosong Yang, Beichen Zhang, Binyuan Hui, Bo Zheng, Bowen Yu, Chengyuan Li, Dayiheng Liu, Fei Huang, Haoran Wei, Huan Lin, Jian Yang, Jianhong Tu, Jianwei Zhang, Jianxin Yang, Jiaxi Yang, Jingren Zhou,

- Junyang Lin, Kai Dang, Keming Lu, Keqin Bao, Kexin Yang, Le Yu, Mei Li, Mingfeng Xue, Pei Zhang, Qin Zhu, Rui Men, Runji Lin, Tianhao Li, Tianyi Tang, Tingyu Xia, Xingzhang Ren, Xuancheng Ren, Yang Fan, Yang Su, Yichang Zhang, Yu Wan, Yuqiong Liu, Zeyu Cui, Zhenru Zhang, and Zihan Qiu. Qwen2.5 technical report. *arXiv*, 2412.15115, 2025. 1, 2, 3, 6, 7, 8, 9, 10
- [92] Alec Radford and Karthik Narasimhan. Improving language understanding by generative pre-training. *OpenAI*, 2018. 1
- [93] Alec Radford, Jeffrey Wu, Rewon Child, David Luan, Dario Amodei, and Ilya Sutskever. Language models are unsupervised multitask learners. *OpenAI*, 2019. 1
- [94] Alec Radford, Jong Wook Kim, Chris Hallacy, Aditya Ramesh, Gabriel Goh, Sandhini Agarwal, Girish Sastry, Amanda Askell, Pamela Mishkin, Jack Clark, Gretchen Krueger, and Ilya Sutskever. Learning transferable visual models from natural language supervision. In *ICML*, 2021. 1, 3, 5, 6, 8, 2, 7, 9, 10, 11
- [95] Sainandan Ramakrishnan, Aishwarya Agrawal, and Stefan Lee. Overcoming language priors in visual question answering with adversarial regularization. In *NeurIPS*, 2018. 1
- [96] Anna Rohrbach, Lisa Anne Hendricks, Kaylee Burns, Trevor Darrell, and Kate Saenko. Object hallucination in image captioning. In *EMNLP*, 2018. 1
- [97] Oriane Siméoni, Huy V. Vo, Maximilian Seitzer, Federico Baldassarre, Maxime Oquab, Cijo Jose, Vasil Khalidov, Marc Szafraniec, Seungeun Yi, Michaël Ramamonjisoa, Francisco Massa, Daniel Haziza, Luca Wehrstedt, Jianyuan Wang, Timothée Darcet, Théo Moutakanni, Leonel Sentana, Claire Roberts, Andrea Vedaldi, Jamie Tolan, John Brandt, Camille Couprie, Julien Mairal, Hervé Jegou, Patrick Labatut, and Piotr Bojanowski. Dinov3. *arXiv*, 2508.10104, 2025. 1, 3, 5, 8, 2, 4, 7, 10
- [98] Amanpreet Singh, Vivek Natarajan, Meet Shah, Yu Jiang, Xinlei Chen, Dhruv Batra, Devi Parikh, and Marcus Rohrbach. Towards vqa models that can read. In *CVPR*, 2019. 2, 6, 7, 10
- [99] Jianlin Su, Murtadha Ahmed, Yu Lu, Shengfeng Pan, Wen Bo, and Yunfeng Liu. Roformer: Enhanced transformer with rotary position embedding. *Neurocomputing*, 2024. 5
- [100] Mirac Suzgun, Nathan Scales, Nathanael Schärli, Sebastian Gehrmann, Yi Tay, Hyung Won Chung, Aakanksha Chowdhery, Quoc V. Le, Ed H. Chi, Denny Zhou, and Jason Wei. Challenging big-bench tasks and whether chain-of-thought can solve them. In *ACL*, 2023. 11
- [101] Hao Tang, Chenwei Xie, Haiyang Wang, Xiaoyi Bao, Tingyu Weng, Pandeng Li, Yun Zheng, and Liwei Wang. Ufo: A unified approach to fine-grained visual perception via open-ended language interface. In *NeurIPS*, 2025. 3, 7, 8
- [102] Shengbang Tong, Ellis Brown, Penghao Wu, Sanghyun Woo, Manoj Middepogu, Sai Charitha Akula, Jihan Yang, Shusheng Yang, Adithya Iyer, Xichen Pan, Austin Wang, Rob Fergus, Yann LeCun, and Saining Xie. Cambrian-1: a fully open, vision-centric exploration of multimodal llms. In *NeurIPS*, 2024. 1, 2, 3, 6, 7, 8, 11
- [103] Shengbang Tong, Zhuang Liu, Yuexiang Zhai, Yi Ma, Yann LeCun, and Saining Xie. Eyes Wide Shut? Exploring the Visual Shortcomings of Multimodal LLMs. In *CVPR*, 2024. 1, 2, 3, 6, 7, 8, 11, 12
- [104] Hugo Touvron, Matthieu Cord, Matthijs Douze, Francisco Massa, Alexandre Sablayrolles, and Herve Jegou. Training data-efficient image transformers and distillation through attention. In *ICML*, 2021. 2, 3
- [105] Hugo Touvron, Thibaut Lavril, Gautier Izacard, Xavier Martinet, Marie-Anne Lachaux, Timothée Lacroix, Baptiste Rozière, Naman Goyal, Eric Hambro, Faisal Azhar, Aurelien Rodriguez, Armand Joulin, Edouard Grave, and Guillaume Lample. Llama: Open and efficient foundation language models. *arXiv*, 2302.13971, 2023. 1, 3, 5
- [106] Michael Tschannen, Alexey Gritsenko, Xiao Wang, Muhammad Ferjad Naeem, Ibrahim Alabdulmohsin, Nikhil Parthasarathy, Talfan Evans, Lucas Beyer, Ye Xia, Basil Mustafa, Olivier Hénaff, Jeremiah Harmsen, Andreas Steiner, and Xiaohua Zhai. Siglip 2: Multilingual vision-language encoders with improved semantic understanding, localization, and dense features. *arXiv*, 2502.14786, 2025. 1, 2, 3, 6, 8, 9, 10, 11
- [107] Laurens van der Maaten and Geoffrey Hinton. Visualizing data using t-sne. *JMLR*, 2008. 8
- [108] Ashish Vaswani, Noam Shazeer, Niki Parmar, Jakob Uszkoreit, Llion Jones, Aidan N. Gomez, Lukasz Kaiser, and Illia Polosukhin. Attention is all you need. In *NeurIPS*, 2017. 5
- [109] Constantin Venhoeff, Ashkan Khazdar, Sonia Joseph, Philip Torr, and Neel Nanda. How visual representations map to language feature space in multimodal llms. *arXiv*, 2506.11976, 2025. 2
- [110] Ali Vosoughi, Shijian Deng, Songyang Zhang, Yapeng Tian, Chenliang Xu, and Jiebo Luo. Cross modality bias in visual question answering: A causal view with possible worlds vqa. *IEEE TMM*, 2024. 1
- [111] Haochen Wang, Yucheng Zhao, Tiancai Wang, Haoqiang Fan, Xiangyu Zhang, and Zhaoxiang Zhang. Ross3d: Reconstructive visual instruction tuning with 3d-awareness. In *ICCV*, 2025. 2, 3
- [112] Haochen Wang, Anlin Zheng, Yucheng Zhao, Tiancai Wang, Zheng Ge, Xiangyu Zhang, and Zhaoxiang Zhang. Reconstructive visual instruction tuning. In *ICLR*, 2025. 2, 3, 8, 6, 7
- [113] Peng Wang, Shuai Bai, Sinan Tan, Shijie Wang, Zhihao Fan, Jinze Bai, Keqin Chen, Xuejing Liu, Jialin Wang, Wenbin Ge, Yang Fan, Kai Dang, Mengfei Du, Xuancheng Ren, Rui Men, Dayiheng Liu, Chang Zhou, Jingren Zhou, and Junyang Lin. Qwen2-vl: Enhancing vision-language model’s perception of the world at any resolution. *arXiv*, 2409.12191, 2024. 5
- [114] Xintong Wang, Jingheng Pan, Liang Ding, and Chris Bie-mann. Mitigating hallucinations in large vision-language models with instruction contrastive decoding. In *ACL*, 2024. 1
- [115] Yunnan Wang, Fan Lu, Kecheng Zheng, Ziyuan Huang, Ziqiang Li, Wenjun Zeng, and Xin Jin. Vision-centric

- activation and coordination for multimodal large language models. *arXiv*, 2510.14349, 2025. 3
- [116] Luis Wiedmann, Orr Zohar, Amir Mahla, Xiaohan Wang, Rui Li, Thibaud Frere, Leandro von Werra, Aritra Roy Gosthipaty, and Andrés Marafioti. Finevision: Open data is all you need. *arXiv*, 2510.17269, 2025. 6, 7
- [117] Huyu Wu, Meng Tang, Xinhan Zheng, and Haiyun Jiang. When language overrules: Revealing text dominance in multimodal large language models. *arXiv*, 2508.10552, 2025. 1
- [118] Penghao Wu, Yushan Zhang, Haiwen Diao, Bo Li, Lewei Lu, and Ziwei Liu. Visual jigsaw post-training improves mllms. *arXiv*, 2509.25190, 2025. 3
- [119] An Yang, Baosong Yang, Binyuan Hui, Bo Zheng, Bowen Yu, Chang Zhou, Chengpeng Li, Chengyuan Li, Dayiheng Liu, Fei Huang, Guanting Dong, Haoran Wei, Huan Lin, Jialong Tang, Jialin Wang, Jian Yang, Jianhong Tu, Jianwei Zhang, Jianxin Ma, Jianxin Yang, Jin Xu, Jingren Zhou, Jinze Bai, Jinzheng He, Junyang Lin, Kai Dang, Keming Lu, Keqin Chen, Kexin Yang, Mei Li, Mingfeng Xue, Na Ni, Pei Zhang, Peng Wang, Ru Peng, Rui Men, Ruize Gao, Runji Lin, Shijie Wang, Shuai Bai, Sinan Tan, Tianhang Zhu, Tianhao Li, Tianyu Liu, Wenbin Ge, Xiaodong Deng, Xiaohuan Zhou, Xingzhang Ren, Xinyu Zhang, Xipin Wei, Xuancheng Ren, Xuejing Liu, Yang Fan, Yang Yao, Yichang Zhang, Yu Wan, Yunfei Chu, Yuqiong Liu, Zeyu Cui, Zhenru Zhang, Zhifang Guo, and Zhihao Fan. Qwen2 technical report. *arXiv*, 2407.10671, 2024. 1, 3, 8
- [120] An Yang, Anfeng Li, Baosong Yang, Beichen Zhang, Binyuan Hui, Bo Zheng, Bowen Yu, Chang Gao, Chenggen Huang, Chenxu Lv, Chujie Zheng, Dayiheng Liu, Fan Zhou, Fei Huang, Feng Hu, Hao Ge, Haoran Wei, Huan Lin, Jialong Tang, Jian Yang, Jianhong Tu, Jianwei Zhang, Jianxin Yang, Jiaxi Yang, Jing Zhou, Jingren Zhou, Junyang Lin, Kai Dang, Keqin Bao, Kexin Yang, Le Yu, Lianghao Deng, Mei Li, Mingfeng Xue, Mingze Li, Pei Zhang, Peng Wang, Qin Zhu, Rui Men, Ruize Gao, Shixuan Liu, Shuang Luo, Tianhao Li, Tianyi Tang, Wenbiao Yin, Xingzhang Ren, Xinyu Wang, Xinyu Zhang, Xuancheng Ren, Yang Fan, Yang Su, Yichang Zhang, Yinger Zhang, Yu Wan, Yuqiong Liu, Zekun Wang, Zeyu Cui, Zhenru Zhang, Zhipeng Zhou, and Zihan Qiu. Qwen3 technical report. *arXiv*, 2505.09388, 2025. 1, 3
- [121] Huanjin Yao, Wenhao Wu, Taojiannan Yang, YuXin Song, Mengxi Zhang, Haocheng Feng, Yifan Sun, Zhiheng Li, Wanli Ouyang, and Jingdong Wang. Dense connector for MLLMs. In *NeurIPS*, 2024. 3
- [122] Hao Yin, Guangzong Si, and Zilei Wang. ClearSight: Visual signal enhancement for object hallucination mitigation in multimodal large language models. *arXiv*, 2503.13107, 2025. 2
- [123] Heeji Yoon, Jaewoo Jung, Junwan Kim, Hyungyu Choi, Heeseong Shin, Sangbeom Lim, Honggyu An, Chaehyun Kim, Jisang Han, Donghyun Kim, Chanho Eom, Sunghwan Hong, and Seungryong Kim. Visual representation alignment for multimodal large language models. *arXiv*, 2509.07979, 2025. 3
- [124] Licheng Yu, Patrick Poirson, Shan Yang, Alexander C. Berg, and Tamara L. Berg. Modeling context in referring expressions. In *ECCV*, 2016. 7
- [125] Xiang Yue, Yuansheng Ni, Kai Zhang, Tianyu Zheng, Ruqi Liu, Ge Zhang, Samuel Stevens, Dongfu Jiang, Weiming Ren, Yuxuan Sun, Cong Wei, Botao Yu, Ruibin Yuan, Renliang Sun, Ming Yin, Boyuan Zheng, Zhenzhu Yang, Yibo Liu, Wenhao Huang, Huan Sun, Yu Su, and Wenhao Chen. Mmmu: A massive multi-discipline multimodal understanding and reasoning benchmark for expert agi. In *CVPR*, 2024. 6, 7
- [126] Xiaohua Zhai, Basil Mustafa, Alexander Kolesnikov, and Lucas Beyer. Sigmoid loss for language image pre-training. In *ICCV*, 2023. 1, 3, 5, 8, 7
- [127] Jiarui Zhang, Mahyar Khayatkhoei, Prateek Chhikara, and Filip Ilievski. Mllms know where to look: Training-free perception of small visual details with multimodal llms. In *ICLR*, 2025. 3
- [128] Xiaofeng Zhang, Yihao Quan, Chen Shen, Xiaosong Yuan, Shaotian Yan, Liang Xie, Wenxiao Wang, Chaochen Gu, Hao Tang, and Jieping Ye. From redundancy to relevance: Information flow in LVLMS across reasoning tasks. In *NAACL*, 2025. 2
- [129] YiFan Zhang, Yang Shi, Weichen Yu, Qingsong Wen, Xue Wang, Wenjing Yang, Zhang Zhang, Liang Wang, and Rong Jin. Debiasing multimodal large language models via penalization of language priors. In *ACM MM*, 2025. 1, 3
- [130] Zhuosheng Zhang, Aston Zhang, Mu Li, Hai Zhao, George Karypis, and Alex Smola. Multimodal chain-of-thought reasoning in language models. *arXiv*, 2302.00923, 2023. 1, 3
- [131] Zefeng Zhang, Hengzhu Tang, Jiawei Sheng, Zhenyu Zhang, Yiming Ren, Zhenyang Li, Dawei Yin, Duohe Ma, and Tingwen Liu. Debiasing multimodal large language models via noise-aware preference optimization. In *CVPR*, 2025. 3
- [132] Zijia Zhao, Longteng Guo, Xingjian He, Shuai Shao, Zehuan Yuan, and Jing Liu. Mamo: Fine-grained vision-language representations learning with masked multimodal modeling. In *ACM SIGIR*, 2023. 3
- [133] Lianmin Zheng, Wei-Lin Chiang, Ying Sheng, Siyuan Zhuang, Zhaghao Wu, Yonghao Zhuang, Zi Lin, Zhuohan Li, Dacheng Li, Eric Xing, Hao Zhang, Joseph E. Gonzalez, and Ion Stoica. Judging LLM-as-a-judge with MT-bench and chatbot arena. In *NeurIPS*, 2023. 9, 11
- [134] Xu Zheng, Chenfei Liao, Yuqian Fu, Kaiyu Lei, Yuanhuiyi Lyu, Lutao Jiang, Bin Ren, Jiale Chen, Jiawen Wang, Chengxin Li, Linfeng Zhang, Danda Pani Paudel, Xuanjing Huang, Yu-Gang Jiang, Nicu Sebe, Dacheng Tao, Luc Van Gool, and Xuming Hu. Mllms are deeply affected by modality bias. *arXiv*, 2505.18657, 2025. 1, 2, 3
- [135] Bolei Zhou, Hang Zhao, Xavier Puig, Sanja Fidler, Adela Barriuso, and Antonio Torralba. Scene parsing through ade20k dataset. In *CVPR*, 2017. 7, 8
- [136] Jinghao Zhou, Chen Wei, Huiyu Wang, Wei Shen, Cihang Xie, Alan Yuille, and Tao Kong. ibot: Image bert pre-training with online tokenizer. *ICLR*, 2022. 2, 3, 4, 5, 1, 6

- [137] Jeffrey Zhou, Tianjian Lu, Swaroop Mishra, Siddhartha Brahma, Sujoy Basu, Yi Luan, Denny Zhou, and Le Hou. Instruction-following evaluation for large language models. *arXiv*, 2311.07911, 2023. [11](#)
- [138] Bin Zhu, Bin Lin, Munan Ning, Yang Yan, Jiaxi Cui, HongFa Wang, Yatian Pang, Wenhao Jiang, Junwu Zhang, Zongwei Li, Wancai Zhang, Zhifeng Li, Wei Liu, and Li Yuan. Languagebind: Extending video-language pretraining to n-modality by language-based semantic alignment. In *ICLR*, 2024. [2](#)

Unleashing the Intrinsic Visual Representation Capability of Multimodal Large Language Models

Supplementary Material

A. Additional Preliminaries

Masked Image Modeling. Masked Image Modeling (MIM) is a self-supervised learning paradigm wherein a model learns to reconstruct representations of masked image regions. Following iBOT [136], an input image I is partitioned into N patches and encoded via a vision encoder \mathcal{G}_ξ . A binary mask $\mathcal{M} \in \{0, 1\}^N$ indicates which patches are masked. iBOT employs a teacher-student framework where the student predicts the teacher’s representations at masked positions. The objective minimizes the cross-entropy between student predictions and teacher targets:

$$\mathcal{L}_{\text{MIM}} = - \sum_{i \in \mathcal{P}_{\mathcal{M}}} \text{softmax}(\hat{\mathbf{z}}_i / \tau_{\text{tea.}}) \cdot \log \text{softmax}(\tilde{\mathbf{z}}_i / \tau_{\text{stu.}}), \quad (10)$$

where $\mathcal{P}_{\mathcal{M}} = \{i \in \{1, \dots, N\} \mid \mathcal{M}_i = 1\}$ denotes the masked position indices, and $\tau_{\text{tea.}}, \tau_{\text{stu.}}$ are temperature parameters controlling the softmax sharpness for teacher and student distributions, respectively. We adopt $\tau_{\text{tea.}} = 0.04$ and $\tau_{\text{stu.}} = 0.1$ by default. This formulation enables the student to learn discriminative semantic representations through reconstruction of masked region features.

CKNNA. *Centered Kernel Nearest-Neighbor Alignment* (CKNNA) [50] is a metric for measuring feature alignment between models, derived as a relaxed variant of *Centered Kernel Alignment* (CKA) [54]. Given two feature sets, CKA quantifies their global similarity through kernel matrices as:

$$\text{CKA}(\mathbf{K}, \mathbf{L}) = \frac{\text{HSIC}(\mathbf{K}, \mathbf{L})}{\sqrt{\text{HSIC}(\mathbf{K}, \mathbf{K})\text{HSIC}(\mathbf{L}, \mathbf{L})}}, \quad (11)$$

where \mathbf{K} and \mathbf{L} denote kernel matrices computed from the feature sets, and $\text{HSIC}(\cdot, \cdot)$ represents the Hilbert-Schmidt Independence Criterion measuring feature dependence. The kernel matrices are defined as $\mathbf{K}_{ij} = \kappa(\mathbf{k}_i, \mathbf{k}_j)$ and $\mathbf{L}_{ij} = \kappa(\mathbf{l}_i, \mathbf{l}_j)$, where $\kappa(\cdot, \cdot)$ is the kernel function and $\mathbf{k}_i, \mathbf{l}_i$ are feature vectors. Using the inner product kernel, HSIC is formulated as:

$$\text{HSIC}(\mathbf{K}, \mathbf{L}) = \frac{1}{(N-1)^2} \left(\sum_{i=1}^N \sum_{j=1}^N (\langle \mathbf{k}_i, \mathbf{k}_j \rangle - \mathbb{E}[\langle \mathbf{k}_i, \mathbf{k}_j \rangle]) (\langle \mathbf{l}_i, \mathbf{l}_j \rangle - \mathbb{E}[\langle \mathbf{l}_i, \mathbf{l}_j \rangle]) \right). \quad (12)$$

CKNNA refines CKA by restricting alignment to nearest

neighbors, replacing $\text{HSIC}(\cdot, \cdot)$ with $\text{HSIC}_{\text{kNN}}(\cdot, \cdot)$:

$$\text{HSIC}_{\text{kNN}}(\mathbf{K}, \mathbf{L}) = \frac{1}{(N-1)^2} \left(\sum_{i=1}^N \sum_{j=1}^N \mathbb{I}(i, j) (\langle \mathbf{k}_i, \mathbf{k}_j \rangle - \mathbb{E}[\langle \mathbf{k}_i, \mathbf{k}_j \rangle]) (\langle \mathbf{l}_i, \mathbf{l}_j \rangle - \mathbb{E}[\langle \mathbf{l}_i, \mathbf{l}_j \rangle]) \right), \quad (13)$$

where $\mathbb{I}(i, j)$ is the nearest-neighbor indicator:

$$\mathbb{I}(i, j) = \begin{cases} 1 & \text{if } i \neq j, \mathbf{k}_i \in \text{kNN}(\mathbf{l}_j; k), \mathbf{l}_j \in \text{kNN}(\mathbf{k}_i; k), \\ 0 & \text{otherwise,} \end{cases} \quad (14)$$

with $\text{kNN}(\mathbf{x}; k)$ denoting the k -nearest neighbors of \mathbf{x} . We set $k = 10$ by default.

B. Additional Discussion on Visual Feature Homogenization

MLLMs exhibit *modality imbalance* [15, 129, 134], systematically biasing toward textual information over visual inputs [51, 57, 73, 88, 129, 134], with more allocated attention scores and predictions predominantly grounded in text modality [88, 117].

To further validate the *progressive visual feature homogenization* phenomenon illustrated in Fig. 2 of the main text, we conduct comprehensive empirical analyses across multiple vision encoders and evaluation metrics. This phenomenon reveals a critical insight: MLLMs progressively discard rich visual information throughout their layers, potentially retaining only those visual features directly relevant to textual reasoning tasks. We posit that this mechanism fundamentally stems from the *next-text-token-prediction* objective, which inherently emphasizes the text modality and provides only indirect, implicit supervisory signals for developing intrinsic visual modeling capabilities. While this text-centric training paradigm proves effective for tasks demanding sophisticated language generation competence, it is suboptimal for training MLLMs that should seamlessly integrate multimodal information without disproportionately favoring any particular modality [22, 103]. The limited performance of MLLMs on dense visual understanding tasks serves as compelling evidence of this text-modality bias.

We provide extensive empirical validation of the *progressive visual feature homogenization* phenomenon in Fig. 7, Fig. 8, and Fig. 9, examining diverse vision encoders including Qwen2.5-7B-Instruct [91] paired with SigLIP

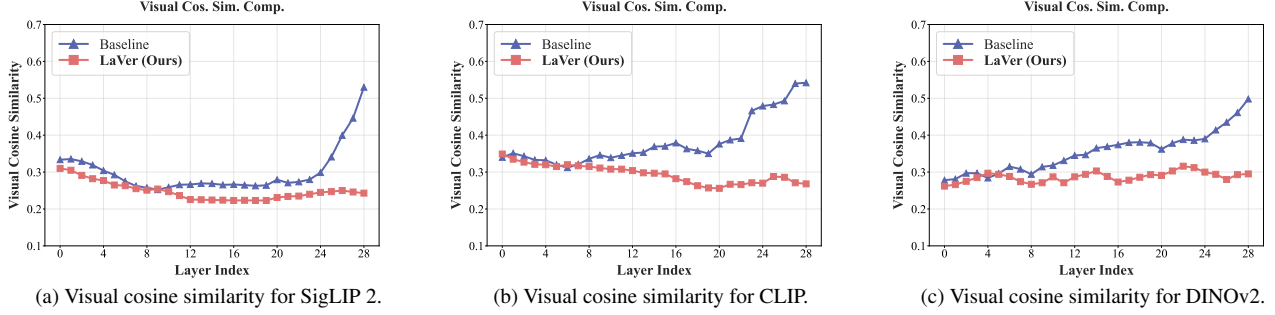


Figure 7. **Averaged visual cosine similarity across the layers.** (a) shows the visual cosine similarity for SigLIP 2 [106]. (b) shows the visual cosine similarity for CLIP [94]. (c) shows the visual cosine similarity for DINOv2 [87].

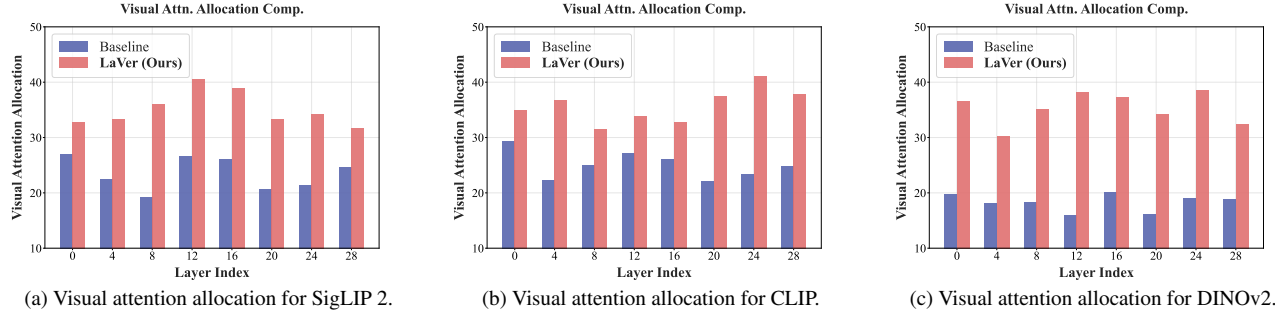


Figure 8. **Averaged visual attention allocation across the layers.** (a) shows the visual attention allocation for SigLIP 2 [106]. (b) shows the visual attention allocation for CLIP [94]. (c) shows the visual attention allocation for DINOv2 [87].

2 [106], CLIP [94], and DINOv2 [87], demonstrating that this phenomenon persists across different architectural configurations. Specifically, we employ the CKNN metric to quantify feature alignment between intermediate visual representations and input visual features, with detailed formulation provided in Sec. A. We construct visual feature sets using images from MMVP [103] and set $k = 10$ as the default neighborhood size.

Our results reveal several critical observations. First, visual feature homogenization intensifies in deeper layers, as evidenced by the progressively increasing averaged visual feature-wise cosine similarity shown in Fig. 7. Second, the substantially diminished visual attention allocation illustrated in Fig. 8 demonstrates that models predominantly leverage information from text tokens, leaving abundant visual information severely underutilized. Notably, our empirical findings indicate that this underutilization of visual information persists consistently across all layers. Third, the gradually decreasing CKNN metric depicted in Fig. 9 indicates progressive misalignment of intermediate visual features from their original representations. In stark contrast to the lower CKNN similarity exhibited by baseline models, our proposed LaVer consistently maintains substantially higher CKNN similarity scores. This demonstrates that LaVer effectively enables models to preserve rich visual information from vision encoders and cultivate

robust intrinsic visual modeling capabilities.

The comprehensive evaluation across diverse benchmarks conclusively demonstrates that by introducing explicit vision-centric supervisory signals, models’ multi-modal capabilities can be significantly enhanced, particularly on tasks demanding dense visual information comprehension and fine-grained visual understanding.

C. Additional Discussion on Visual Feature Inconsistency

As demonstrated in Sec. 4.2, applying the Masked Image Modeling (MIM) objective in isolation paradoxically leads to increased visual cosine similarity, signaling severe visual information degradation rather than enhancement. Our analysis of training dynamics reveals a critical pattern: while visual cosine similarity initially decreases during early training iterations, it rapidly escalates in subsequent phases, ultimately surpassing baseline levels. This counterintuitive behavior arises because the MIM objective, while encouraging the model to reconstruct its own visual embeddings, fails to explicitly constrain the model from generating homogeneous visual features, i.e., a degenerate solution that minimizes MIM loss at the expense of preserving meaningful visual distinctions.

This phenomenon bears striking resemblance to observations reported in prior work [17, 87, 97], where models

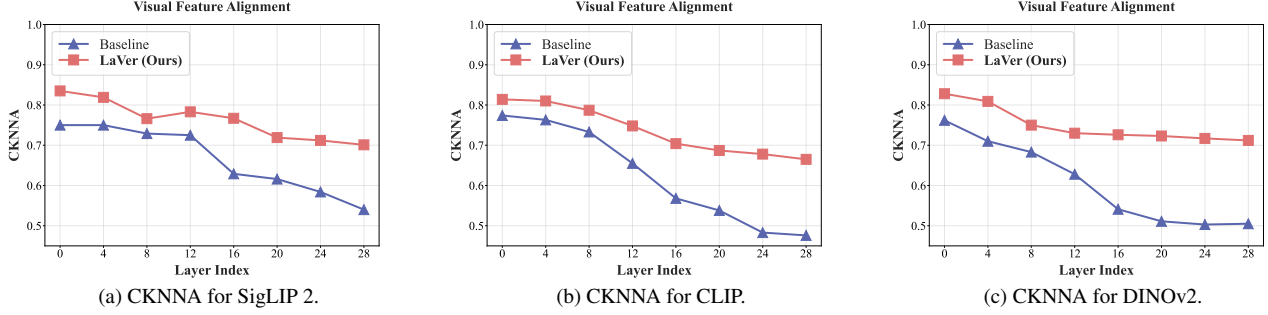


Figure 9. **CKNNA metrics across the layers.** (a) displays the CKNNA metric for SigLIP 2 [106]. (b) displays the CKNNA metric for CLIP [94]. (c) displays the CKNNA metric for DINOv2 [87].

Table 4. **Hyperparameters of training stages.**

Configuration	Stage 1	Stage 2	Stage 3
Trainable parameters	Connector \mathcal{H}_ϕ	Connector \mathcal{H}_ϕ , LLM \mathcal{F}_θ , Vision Head \mathcal{V}_ψ	Connector \mathcal{H}_ϕ , LLM \mathcal{F}_θ
Frozen parameters	Vision Encoder \mathcal{G}_ξ , LLM \mathcal{F}_θ	Vision Encoder \mathcal{G}_ξ , Teacher LLM \mathcal{F}_θ , Teacher Vision Head \mathcal{V}_ψ	Vision Encoder \mathcal{G}_ξ
Global batch size	128	128	128
Batch size per GPU	4	2	4
Accumulation steps	2	4	2
Max sequence length	2048	2048	2048
DeepSpeed Zero Stage	2	2	2
Learning rate	2.0×10^{-3}	2.0×10^{-5}	1.0×10^{-5}
Learning rate schedule	Cosine	Cosine	Cosine
Warmup ratio	0.05	0.05	0.05
Weight decay	0	0	0
Training steps	4360	6250	6250
Data scale	558K	800K	800K
Optimizer	AdamW	AdamW	AdamW
β_1, β_2	0.9, 0.999	0.9, 0.999	0.9, 0.999
Precision	bf16	bf16	bf16

Table 5. **Hyperparameters of LaVer.**

Configuration	LaVer
Visual hidden dimension	8192
Loss coefficient ω_{MIM}	1.0
Loss coefficient ω_{CGA}	1.0
Teacher temperature τ_{tea}	0.04
Student temperature τ_{stu}	0.1
Masking ratio	0.05
Masking schedule	Cosine
EMA decay rate	0.95
EMA update steps	100
EMA schedule	Cosine

progressively generate visual features exhibiting high cosine similarity with global semantic tokens while discarding fine-grained local structural information. Given the conceptual alignment between our observations under isolated MIM training and these established findings, we adopt the terminology *visual feature inconsistency* to characterize this pathology, wherein visual patches exhibit spuriously high cosine similarity despite encoding fundamentally distinct

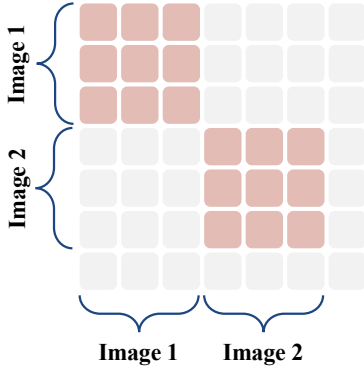
Table 6. **Hyperparameters of ReasonSeg.**

Configuration	ReasonSeg
Trainable parameters	Connector \mathcal{H}_ϕ , LLM \mathcal{F}_θ
Frozen parameters	Vision Encoder \mathcal{G}_ξ
Global batch size	128
Batch size per GPU	4
Accumulation steps	2
Max sequence length	2048
DeepSpeed Zero Stage	2
Learning rate	2.0×10^{-4}
Learning rate schedule	Cosine
Warmup ratio	0.01
Weight decay	0.01
Training steps	30000
Data scale	3.8M
Optimizer	AdamW
β_1, β_2	0.9, 0.999
Precision	bf16

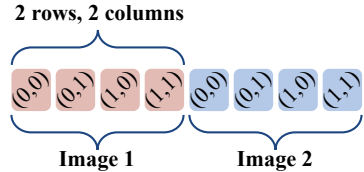
local visual information. While this phenomenon was attributed to the global semantic contrastive loss in the DINO series [97], our empirical findings reveal that local MIM

Table 7. **Computational cost comparison of stage 2.** LaVer introduces modest computational overhead compared to the baseline, with training time increases of 13-16% and memory consumption increases of 14-26% across different vision encoders. Despite these additional costs, the substantial performance improvements demonstrated in our experiments justify this overhead, making LaVer a practical and effective approach for enhancing MLLM capabilities.

Vision encoder	Method	Trainable Parameters	Training Speed	Training Time	Total GFLOPs	Memory Consumption
SigLIP 2	Baseline	7.63B	4.87 s/iter	8 h 27 min	2.46×10^{10}	55.24 GB
	LaVer	7.65B	5.51 s/iter	9 h 34 min	3.04×10^{10}	69.82 GB
CLIP	Baseline	7.63B	4.23 s/iter	7 h 42 min	2.24×10^{10}	53.24 GB
	LaVer	7.65B	4.67 s/iter	8 h 28 min	2.80×10^{10}	66.79 GB
DINOv2	Baseline	7.63B	3.98 s/iter	6 h 55 min	1.85×10^{10}	51.24 GB
	LaVer	7.65B	4.45 s/iter	7 h 44 min	2.19×10^{10}	58.24 GB



(a) Diagonally blocked full attention.



(b) Blocked 2D-RoPE.

Figure 10. **Illustration of packed visual sequences.** (a) illustrates diagonally blocked full attention for packed visual sequence. (b) illustrates blocked 2D-RoPE for packed visual sequence.

objectives can independently induce the same degenerative behavior, highlighting a new failure mode.

To address this challenge, the *Gram-Anchoring* mechanism was proposed by [97] to explicitly enforce preservation of spatial structural information while learning discriminative local embeddings for each patch. However, *Gram-Anchoring* exhibits a fundamental limitation: it symmetrically penalizes deviations in both directions, thereby inadvertently discouraging the emergence of discriminative visual features. Specifically, when the model attempts to produce more distinctive representations characterized by lower feature-wise cosine similarity, it incurs penalties equivalent to those for generating overly homogeneous features. While this symmetric regularization proves benign for vision-only models [97], it becomes problematic in the context of MLLMs, which inherently suffer from modality imbalance. The pre-existing bias toward textual modal-

ity creates a perverse incentive: the model can exploit this imbalance by generating nearly identical visual features to trivially minimize the MIM objective, effectively circumventing genuine visual understanding.

To overcome this limitation, we propose *Clipped Gram-Anchoring*, an asymmetric regularization strategy that selectively penalizes the model only when it tends to produce visual features with excessively high cosine similarity. By imposing penalties exclusively on the homogenization direction while permitting the model to freely explore more discriminative feature spaces, this regularizer effectively prevents visual feature inconsistency. This design aligns with the fundamental requirement for MLLMs, i.e., maintaining rich, discriminative visual representations that can meaningfully contribute to multimodal reasoning, rather than collapsing into degenerate solutions that superficially satisfy training objectives while sacrificing genuine visual understanding capabilities.

Visual Feature Homogenization v.s. Visual Feature Inconsistency. To elucidate the fundamental distinctions between these two phenomena, we provide a justification of their divergent characteristics. While both *visual feature homogenization* and *visual feature inconsistency* manifest the same statistical signature, namely, the generation of visual features exhibiting elevated feature-wise cosine similarity, their underlying causal mechanisms and downstream implications differ substantially.

Visual feature homogenization emerges as a direct consequence of the modality imbalance inherent in MLLMs’ training paradigm. Under the text-centric next-token-prediction objective, models systematically exploit textual tokens to generate responses while marginalizing the majority of available visual information. This preferential reliance on textual modality precipitates a progressive degradation of visual representations, manifesting as increased homogeneity among visual features across layers. Critically, this phenomenon reflects a fundamental loss of discriminative visual information rather than a mere representational artifact.

In contrast, *visual feature inconsistency* originates from

Table 8. **Scalability of LaVer on model parameters.** LaVer demonstrates strong model scaling properties, consistently improving performance across different parameter sizes (1.5B, 3B, and 7B) with both SigLIP 2 and CLIP vision encoders.

Benchmark	SigLIP2									CLIP								
	1.5B			3B			7B			1.5B			3B			7B		
	Baseline	LaVer	Δ_{Baseline}	Baseline	LaVer	Δ_{Baseline}	Baseline	LaVer	Δ_{Baseline}	Baseline	LaVer	Δ_{Baseline}	Baseline	LaVer	Δ_{Baseline}	Baseline	LaVer	Δ_{Baseline}
GQA	45.98	48.51	$\uparrow 2.53$	48.99	53.02	$\uparrow 4.03$	55.03	56.78	$\uparrow 1.75$	46.98	48.25	$\uparrow 1.27$	50.00	48.99	$\downarrow 1.01$	51.51	54.77	$\uparrow 3.26$
MMB ^{EN}	61.89	65.51	$\uparrow 3.62$	70.79	74.23	$\uparrow 3.44$	73.97	75.60	$\uparrow 1.63$	54.33	60.22	$\uparrow 5.89$	62.80	63.23	$\uparrow 0.43$	68.64	69.93	$\uparrow 1.29$
SEED ^I	58.65	63.04	$\uparrow 4.39$	64.45	66.10	$\uparrow 1.65$	67.57	68.62	$\uparrow 1.05$	56.18	62.22	$\uparrow 6.04$	62.63	62.67	$\uparrow 0.04$	64.36	65.20	$\uparrow 0.84$
MME	1261.35	1285.18	$\uparrow 23.83$	1384.78	1445.33	$\uparrow 60.55$	1510.73	1512.50	$\uparrow 1.77$	1175.37	1213.01	$\uparrow 37.64$	1260.48	1379.26	$\uparrow 118.78$	1289.62	1474.65	$\uparrow 185.03$
RWQA	52.68	52.29	$\downarrow 0.39$	56.08	58.56	$\uparrow 2.48$	53.86	59.35	$\uparrow 5.49$	50.85	52.16	$\uparrow 1.31$	56.73	55.29	$\downarrow 1.44$	54.25	56.47	$\uparrow 2.22$
MMMU	40.11	41.11	$\uparrow 1.00$	41.11	42.00	$\uparrow 0.89$	44.78	46.33	$\uparrow 1.55$	38.33	39.44	$\uparrow 1.11$	42.44	40.67	$\downarrow 1.77$	44.56	44.56	$\uparrow 0.00$
MM*	38.02	40.90	$\uparrow 2.88$	46.80	50.07	$\uparrow 3.27$	49.06	52.01	$\uparrow 2.95$	37.42	40.83	$\uparrow 3.41$	41.97	44.05	$\uparrow 2.08$	43.17	45.45	$\uparrow 2.28$
OCRB	237	258	$\uparrow 21$	353	397	$\uparrow 44$	536	639	$\uparrow 103$	136	162	$\uparrow 26$	226	265	$\uparrow 39$	306	365	$\uparrow 59$
TVQA	42.42	44.96	$\uparrow 2.54$	51.33	55.78	$\uparrow 4.45$	62.06	63.93	$\uparrow 1.87$	31.70	34.65	$\uparrow 2.95$	40.85	48.49	$\uparrow 7.64$	43.86	49.93	$\uparrow 6.07$
CQA	27.84	31.52	$\uparrow 3.68$	40.00	42.32	$\uparrow 2.32$	43.52	50.24	$\uparrow 6.72$	18.40	19.04	$\uparrow 0.64$	26.00	30.52	$\uparrow 4.52$	27.36	39.36	$\uparrow 12.00$
AI2D	59.94	62.56	$\uparrow 2.62$	72.05	75.39	$\uparrow 3.34$	73.74	75.55	$\uparrow 1.81$	59.39	60.46	$\uparrow 1.07$	64.73	65.54	$\uparrow 0.81$	66.00	70.40	$\uparrow 4.40$
MMVP	60.67	63.67	$\uparrow 3.00$	65.00	64.00	$\downarrow 1.00$	69.00	70.33	$\uparrow 1.33$	52.00	54.67	$\uparrow 2.67$	55.00	59.00	$\uparrow 4.00$	60.00	64.00	$\uparrow 4.00$
CV-B ^{2D}	52.69	53.13	$\uparrow 0.44$	58.69	62.80	$\uparrow 4.11$	67.87	69.82	$\uparrow 1.95$	51.95	60.50	$\uparrow 8.55$	57.93	61.17	$\uparrow 3.24$	64.39	65.58	$\uparrow 1.19$
SQA	72.78	76.45	$\uparrow 3.67$	83.75	85.09	$\uparrow 1.34$	86.51	89.09	$\uparrow 2.58$	69.36	76.00	$\uparrow 6.64$	72.73	73.18	$\uparrow 0.45$	81.61	83.30	$\uparrow 1.69$
MathV	35.90	43.10	$\uparrow 7.20$	46.20	50.80	$\uparrow 4.60$	52.20	55.60	$\uparrow 3.40$	34.50	41.30	$\uparrow 6.80$	41.60	43.30	$\uparrow 1.70$	45.40	48.90	$\uparrow 3.50$
Hallu	50.26	52.37	$\uparrow 2.11$	53.99	54.68	$\uparrow 0.69$	56.05	58.04	$\uparrow 1.99$	46.37	48.37	$\uparrow 2.00$	53.89	51.84	$\downarrow 2.05$	53.42	55.95	$\uparrow 2.53$
POPE	86.87	88.67	$\uparrow 1.80$	86.03	85.53	$\downarrow 0.50$	90.90	91.23	$\uparrow 0.33$	86.03	88.60	$\uparrow 2.57$	87.17	90.70	$\uparrow 3.53$	90.50	90.30	$\downarrow 0.20$
Average	46.32	48.74	$\uparrow 2.42$	52.13	54.20	$\uparrow 2.07$	55.72	57.87	$\uparrow 2.15$	43.20	46.32	$\uparrow 3.12$	48.07	49.38	$\uparrow 1.31$	50.58	53.24	$\uparrow 2.66$

Table 9. **Scalability of LaVer on datasets.** LaVer demonstrates strong data scaling properties, consistently improving performance across different training dataset sizes.

Benchmark	SigLIP 2									CLIP								
	800K			2M			4M			800K			2M			4M		
	Baseline	LaVer	Δ_{Baseline}	Baseline	LaVer	Δ_{Baseline}	Baseline	LaVer	Δ_{Baseline}	Baseline	LaVer	Δ_{Baseline}	Baseline	LaVer	Δ_{Baseline}	Baseline	LaVer	Δ_{Baseline}
GQA	55.03	56.78	$\uparrow 1.75$	53.52	58.29	$\uparrow 4.77$	57.54	58.79	$\uparrow 1.25$	51.51	54.77	$\uparrow 3.26$	53.27	55.53	$\uparrow 2.26$	51.01	53.52	$\uparrow 2.51$
MMB ^{EN}	73.97	75.60	$\uparrow 1.63$	74.83	75.69	$\uparrow 0.86$	73.37	76.20	$\uparrow 2.83$	68.64	69.93	$\uparrow 1.29$	68.81	73.02	$\uparrow 4.21$	69.50	76.12	$\uparrow 6.62$
SEED ^I	67.57	68.62	$\uparrow 1.05$	67.11	68.15	$\uparrow 1.04$	67.61	68.02	$\uparrow 0.41$	64.36	65.20	$\uparrow 0.84$	63.66	65.70	$\uparrow 2.04$	64.58	66.97	$\uparrow 2.39$
MME	1510.73	1512.50	$\uparrow 1.77$	1549.66	1589.66	$\uparrow 40.00$	1574.33	1635.16	$\uparrow 60.83$	1289.62	1474.65	$\uparrow 185.03$	1312.79	1390.06	$\uparrow 77.27$	1392.78	1461.37	$\uparrow 68.59$
RWQA	53.86	59.35	$\uparrow 5.49$	60.65	63.53	$\uparrow 2.88$	59.61	63.92	$\uparrow 4.31$	54.25	56.47	$\uparrow 2.22$	54.63	58.04	$\uparrow 3.41$	53.86	59.22	$\uparrow 5.36$
MMMU	44.78	46.33	$\uparrow 1.55$	43.56	45.56	$\uparrow 2.00$	42.89	45.79	$\uparrow 2.90$	44.56	44.56	$\uparrow 0.00$	43.11	44.44	$\uparrow 1.33$	41.00	42.44	$\uparrow 1.44$
MM*	49.06	52.01	$\uparrow 2.95$	50.67	50.74	$\uparrow 0.07$	51.54	52.54	$\uparrow 1.00$	43.17	45.45	$\uparrow 2.28$	46.79	48.85	$\uparrow 2.06$	44.85	50.61	$\uparrow 5.76$
OCRB	536	639	$\uparrow 103$	637	678	$\uparrow 41$	665	684	$\uparrow 19$	306	365	$\uparrow 59$	355	387	$\uparrow 32$	351	400	$\uparrow 49$
TVQA	62.06	63.93	$\uparrow 1.87$	64.93	68.65	$\uparrow 3.72$	67.71	69.11	$\uparrow 1.40$	43.86	49.93	$\uparrow 6.07$	45.65	54.26	$\uparrow 8.61$	52.39	57.73	$\uparrow 5.34$
CQA	43.52	50.24	$\uparrow 6.72$	58.88	64.48	$\uparrow 5.60$	61.44	64.88	$\uparrow 3.44$	27.36	39.36	$\uparrow 12.00$	38.24	45.20	$\uparrow 6.96$	42.84	51.04	$\uparrow 8.20$
AI2D	73.74	75.55	$\uparrow 1.81$	73.44	75.22	$\uparrow 1.78$	73.15	75.06	$\uparrow 1.91$	66.00	70.40	$\uparrow 4.40$	66.65	70.98	$\uparrow 4.33$	67.97	73.39	$\uparrow 5.42$
MMVP	69.00	70.33	$\uparrow 1.33$	67.00	71.33	$\uparrow 4.33$	70.67	72.33	$\uparrow 1.66$	60.00	64.00	$\uparrow 4.00$	62.67	66.33	$\uparrow 3.66$	64.00	69.00	$\uparrow 5.00$
CV-B ^{2D}	67.87	69.82	$\uparrow 1.95$	71.70	71.77	$\uparrow 0.07$	72.11	73.35	$\uparrow 1.24$	64.39	65.58	$\uparrow 1.19$	61.27	64.67	$\uparrow 3.40$	62.94	67.66	$\uparrow 4.72$
SQA	86.51	89.09	$\uparrow 2.58$	81.95	86.47	$\uparrow 4.52$	84.28	87.01	$\uparrow 2.73$	81.61	83.30	$\uparrow 1.69$	83.89	84.83	$\uparrow 0.94$	84.79	90.88	$\uparrow 6.09$
MathV	52.20	55.60	$\uparrow 3.40$	53.10	56.70	$\uparrow 3.60$	53.50	56.70	$\uparrow 3.20$	45.40	48.90	$\uparrow 3.50$	47.00	51.70	$\uparrow 4.70$	49.90	56.70	$\uparrow 6.80$
Hallu	56.05	58.04	$\uparrow 1.99$	60.15	61.41	$\uparrow 1.26$	58.36	60.99	$\uparrow 2.63$	53.42	55.95	$\uparrow 2.53$	56.20	57.41	$\uparrow 1.21$	57.52	56.89	$\downarrow 0.63$
POPE	90.90	91.23	$\uparrow 0.33$	91.33	91.47	$\uparrow 0.14$	92.23	91.93	$\downarrow 0.30$	90.50	90.30	$\downarrow 0.20$	88.47	90.97	$\uparrow 2.50$	90.13	89.07	$\downarrow 1.06$
Average	55.72	57.87	$\uparrow 2.15$	57.30	59.46	$\uparrow 2.16$	58.08	59.88	$\uparrow 1.80$	50.58	53.24	$\uparrow 2.66$	51.84	54.88	$\uparrow 3.04$	52.84	56.60	$\uparrow 3.77$

the explicit application of the MIM objective in isolation. While MIM provides direct supervisory signals that guide the evolution of visual embeddings, it simultaneously introduces an exploitable optimization shortcut: the model can trivially minimize MIM loss by generating nearly identical visual features, thereby achieving low reconstruction error without preserving meaningful visual distinctions. Consequently, the isolated MIM objective exacerbates rather than ameliorates the situation, failing to provide balanced supervisory signals across modalities and inadvertently reinforcing the collapse toward homogeneous representations.

Our proposed LaVer framework addresses both pathologies synergistically. By integrating the Clipped Gram-Anchoring mechanism with the MIM objective, LaVer effectively prevents visual feature inconsistency through asymmetric regularization that selectively penalizes excessive homogenization while permitting discriminative feature learning. Simultaneously, by introducing explicit vision-centric supervisory signals, LaVer mitigates

the underlying modality imbalance issue, enabling models to maintain rich, discriminative visual representations throughout their layers. This dual-pronged approach culminates in substantially enhanced performance across diverse multimodal benchmarks, particularly on tasks demanding dense visual understanding.

D. Implementation Details

Hyperparameters. We summarize the hyperparameters for each training stage in Table 4. Following common practice in LLaVA-OneVision 1.5 [3], we adopt standard configurations for our three-stage training pipeline. Note that we do not use the exact datasets from LLaVA-OneVision 1.5, as they were not fully available at the time of our experiments. LaVer is applied exclusively to Stage 2, where visual knowledge is injected into the model. The specific hyperparameters of LaVer are detailed in Table 5. We observe that LaVer’s performance is robust to most hyperparameter choices, requiring minimal tuning. Through comprehen-

Table 10. Ablation study on masking strategies. LaVer demonstrates strong robustness across different masking strategies.

Benchmark	SigLIP 2									CLIP								
	Baseline	Cosine				Constant				Baseline	Cosine				Constant			
		0.05	0.1	0.2	0.3	0.0002	0.01	0.05	0.1		0.05	0.1	0.2	0.3	0.0002	0.01	0.05	0.1
GQA	55.03	56.78	56.53	56.26	54.87	54.83	55.96	55.22	56.11	51.51	54.77	54.71	54.52	52.76	52.26	53.02	52.26	51.01
MMB ^{EN}	73.97	75.60	75.65	75.04	73.99	74.89	73.74	74.46	73.80	68.64	69.93	69.24	70.62	71.39	65.38	70.10	72.77	70.27
SEED ^I	67.57	68.62	68.50	68.49	67.48	67.82	68.42	68.34	67.96	64.36	65.20	65.02	64.27	64.99	64.67	64.21	64.81	65.03
MME	1510.73	1512.50	1546.12	1515.43	1534.31	1504.69	1496.10	1532.54	1495.53	1289.62	1474.65	1470.28	1407.86	1404.61	1421.08	1381.88	1399.67	1441.57
RWQA	53.86	59.35	58.77	58.62	55.51	58.33	55.18	54.55	56.17	54.25	56.47	55.59	55.56	54.12	52.42	54.51	55.56	52.94
MMMU	44.78	46.33	46.31	45.96	44.63	44.85	45.77	44.57	45.95	44.56	44.56	45.44	44.11	43.22	41.33	44.89	43.89	43.89
MM*	49.06	52.01	52.04	51.44	50.12	51.31	48.97	50.71	50.95	43.17	45.45	45.31	45.25	47.39	42.30	45.11	45.72	46.12
OCRB	536	639	638	625	582	619	606	607	597	306	365	354	345	301	292	302	300	297
TVQA	62.06	63.93	64.11	63.98	62.07	61.79	63.59	62.37	63.92	43.86	49.93	49.28	48.55	48.78	49.03	48.07	49.05	47.47
CQA	43.52	50.24	46.20	48.49	48.94	46.66	46.52	46.21	48.48	27.36	39.36	36.32	34.00	34.24	33.52	33.20	33.36	33.04
AI2D	73.74	75.55	75.86	74.68	73.61	74.37	73.65	74.35	73.70	66.00	70.40	69.46	68.62	69.59	65.38	70.14	69.95	69.24
MMVP	69.00	70.33	70.33	69.33	69.00	70.00	69.67	69.33	68.33	60.00	64.00	63.67	63.67	62.33	59.33	63.67	61.33	61.33
CV-B ^{2D}	67.87	69.82	68.96	70.06	67.67	68.87	68.68	67.97	68.40	64.39	65.58	65.42	64.26	62.17	60.36	62.38	61.20	62.10
SQA	86.51	89.09	86.11	88.78	88.17	87.09	86.62	86.65	87.45	81.61	83.30	83.29	82.15	82.90	80.47	82.40	82.60	82.30
MathV	52.20	55.60	52.16	55.82	54.32	52.38	51.98	54.26	54.16	45.40	48.90	46.20	45.90	47.70	46.10	46.90	47.10	46.80
Hallu	56.05	58.04	58.29	58.33	56.27	57.72	56.89	57.45	56.61	53.42	55.95	55.95	55.10	51.00	54.26	54.00	54.89	55.63
POPE	90.90	91.23	91.24	90.73	90.51	90.55	90.58	90.49	90.57	90.50	90.30	90.93	90.10	90.43	89.43	89.26	90.00	89.27
Average	55.72	57.87	57.20	57.49	56.38	56.63	56.32	56.36	56.69	50.58	53.24	52.75	52.21	51.99	50.42	51.93	52.08	51.61

Table 11. Ablation study on EMA teacher strategies.

Method	SigLIP 2												CLIP														
	LaVer												LaVer														
	Baseline	Con.	Cos.	Cos.	Cos.	Cos.	Cos.	Cos.	Cos.	Cos.	Cos.	Cos.	Baseline	Con.	Cos.	Cos.	Cos.	Cos.	Cos.	Cos.	Cos.	Cos.	Cos.	Cos.	Cos.	Cos.	
EMA Str.	-	Con.	Cos.	Cos.	Cos.	Cos.	Cos.	Cos.	Cos.	Cos.	Cos.	Cos.	-	Con.	Cos.	Cos.	Cos.	Cos.	Cos.	Cos.	Cos.	Cos.	Cos.	Cos.	Cos.	Cos.	
EMA Freq.	100	100	100	1	50	100	200	100	100	100	100	100	100	100	100	1	50	100	200	100	100	100	100	100	100	100	
EMA Ratio	-	0.95	0.95	0.95	0.95	0.95	0.95	0.95	0.9	0.95	0.99	0.999	-	0.95	0.95	0.95	0.95	0.95	0.95	0.9	0.95	0.99	0.999	0.999	0.999	0.999	
GQA	55.03	55.63	56.78	53.65	55.22	56.78	57.19	56.44	56.78	55.90	56.07	51.51	51.72	54.77	50.91	51.39	54.77	55.03	54.09	54.77	54.00	53.97	55.03	54.09	54.77	54.00	53.97
MMB ^{EN}	73.97	77.39	75.60	70.44	73.70	75.60	73.43	75.21	75.60	75.12	75.70	68.64	70.99	69.93	65.54	70.56	69.93	70.58	71.19	69.93	71.22	69.57	71.22	71.19	69.93	71.22	69.57
SEED ^I	67.57	67.82	68.62	64.39	69.43	68.62	69.49	69.57	68.62	69.16	69.36	64.36	66.71	65.20	61.54	64.43	65.20	65.96	63.81	65.20	66.75	66.92	66.92	63.81	65.20	66.75	66.92
MME	1510.73	1546.52	1512.50	1436.02	1574.55	1512.50	1521.53	1544.95	1512.50	1501.03	1507.67	1289.62	1393.95	1474.65	1361.29	1315.01	1474.65	1366.78	1328.63	1474.65	1462.85	1481.98	1481.98	1328.63	1474.65	1462.85	1481.98
RWQA	53.86	55.56	59.35	55.31	53.34	59.35	56.42	55.90	59.35	56.46	55.91	54.25	55.10	56.47	53.34	54.79	56.47	54.43	56.01	56.47	56.70	55.35	56.70	56.01	56.47	56.70	55.35
MMMU	44.78	45.48	46.33	43.21	45.85	46.33	45.18	44.81	46.33	44.69	44.57	44.56	44.96	44.56	42.33	44.24	44.56	45.43	45.86	44.56	44.89	45.02	45.86	44.56	44.89	45.02	45.86
MM*	49.06	50.49	52.01	49.32	48.84	52.01	50.35	49.36	52.01	51.74	51.93	43.17	44.80	45.45	42.18	45.17	45.45	43.57	45.79	45.45	46.23	46.50	46.50	45.79	45.45	46.23	46.50
OCRB	536	651	639	537	633	639	637	577	639	649	565	306	351	365	298	355	365	357	365	365	337	362	365	337	362	362	362
TVQA	62.06	65.79	63.93	59.38	62.33	63.93	65.27	62.29	63.93	63.97	65.08	43.86	45.39	49.93	46.66	47.42	49.93	45.40	46.76	49.93	46.04	48.64	49.93	46.76	49.93	46.04	48.64
CQA	43.52	47.00	50.24	44.98	45.54	50.24	49.01	47.87	50.24	49.66	47.48	27.36	40.53	39.36	30.08	36.81	39.36	33.66	37.27	39.36	37.22	40.24	37.27	39.36	37.22	40.24	
AI2D	73.74	75.68	75.55	70.87	75.36	75.76	74.53	75.55	75.01	73.38	66.00	65.59	70.40	63.35	65.96	70.40	67.99	68.59	70.40	69.86	69.72	69.72	69.72	68.59	70.40	69.86	69.72
MMVP	69.00	72.67	70.33	66.00	71.00	70.33	72.00	71.33	70.33	72.33	70.67	60.00	62.00	64.00	59.67	64.67	64.00	63.00	62.33	64.00	62.00	63.33	62.33	64.00	62.00	63.33	
CV-B ^{2D}	67.87	69.08	69.82	66.10	70.44	69.82	70.05	67.29	69.82	69.30	69.58	64.39	67.42	65.58	61.70	65.54	65.58	67.09	65.45	65.58	67.52	66.21	67.52	65.45	65.58	67.52	66.21
SQA	86.51	89.59	89.09	82.90	88.33	89.09	87.24	90.41	89.09	86.34	86.86	81.61	85.17	83.30	77.91	84.23	83.30	85.23	82.95	83.30	82.39	82.25	85.23	82.95	83.30	82.39	82.25
MathV	52.20	55.73	52.60	52.46	55.06	55.60	54.23	53.39	55.60	55.68	52.74	45.40	50.01	48.90	45.75	49.20	48.90	47.51	46.63	48.90	47.86	48.47	46.63	48.90	47.86	48.47	
Hallu	56.05	56.72	58.04	54.29	57.15	58.04	56.55	59.46	58.04	59.13	56.13	53.42	57.28	55.95	52.25	55.32	55.95	56.37	53.10	55.95	54.98	56.32	53.10	55.95	54.98	56.32	
POPE	90.90	90.44	91.23	86.37	90.21	91.23	91.64	91.61	91.23	90.07	91.97	90.50	90.96	90.30	85.97	91.77	90.30	92.56	90.03	90.30	91.09	91.68	92.56	90.03	90.30	91.09	91.68
Average	55.72	57.43	57.87	54.17	56.65	57.87	57.36	57.10	57.87	57.40	56.98	50.58	52.92	53.24	49.41	52.49	53.24	52.63	52.40	53.24	52.92	53.25	53.25	52.40	53.24	52.92	53.25

sive ablation studies on masking strategies and EMA updating strategies, we demonstrate LaVer’s robustness to hyperparameter variations. Our findings indicate that a small masking ratio with cosine scheduling is sufficient for effective learning. For EMA updates, we find that the strategy is insensitive to the update schedule as long as the update frequency is not excessively high; overly frequent updates can cause the model to exploit the MIM loss by inadvertently propagating visual feature inconsistencies into the teacher model. For the vision head architecture, we employ a lightweight 3-layer MLP with 8192 hidden dimensions, parallel to the language head. This design introduces only a negligible number of additional trainable parameters. Following the established practice in [136], we set the teacher temperature $\tau_{\text{tea.}} = 0.04$ and student temperature $\tau_{\text{stu.}} = 0.1$, which ensures stable convergence throughout training. For fair comparison with ROSS [112], we adopt their 2-stage training protocol with identical configurations as specified in [112]. All experiments are conducted on 16 NVIDIA A100 GPUs with 80GB memory each.

Datasets. Our training pipeline employs off-the-shelf datasets across three stages. For Stage 1, we adopt

the LLaVA-558K dataset [67] for vision-language alignment. For Stage 2, we randomly sample 800K image-text pairs from FineVision 23M [116], maintaining the original dataset’s proportions to preserve its diverse visual knowledge sources. Due to computational constraints, we do not utilize the complete dataset; however, we validate LaVer’s data scaling properties by sampling up to 4M pairs from FineVision. For Stage 3, we randomly sample 800K instruction-tuning pairs from LLaVA-OneVision 4M [60], again preserving the original proportions. While potential overlap may exist between Stage 2 and Stage 3 data, we retain all samples as this configuration has proven empirically effective. For fair comparison with ROSS [112], we adopt their 2-stage protocol using LLaVA-558K [67] for Stage 1 and Cambrian-737K [102] for Stage 2.

Vision encoders. We evaluate LaVer across diverse vision encoders to demonstrate its broad applicability. SigLIP 2 [106] employs pairwise sigmoid loss instead of softmax for enhanced image-text alignment and multilingual capabilities. For our main experiments, we adopt SigLIP 2-ViT-SO400M/14@384, which encodes 384×384 images into 729 vision tokens. For comparison with

Table 12. Ablation study on spatial awareness.

\mathcal{G}_L	LaVer	Mixed Attn.	2D-RoPE	GQA	MMB ^{EN}	SEED ^I	MME	RWQA	MMMU	MM*	OCRB	TVQA	CQA	AI2D	MMVP	CV-B ^{2D}	SQA	MathV	Hallu	POPE	Avg.
SigLIP 2	✗	✗	✗	55.03	73.97	67.57	1510.73	53.86	44.78	49.06	536	62.06	43.52	73.74	69.00	67.87	86.51	52.20	56.05	90.90	55.72
	✗	✓	✗	54.33	74.98	68.31	1505.55	55.17	45.32	49.54	641	61.40	45.38	75.94	71.00	70.62	88.62	56.05	55.83	91.57	56.78
	✗	✗	✓	54.87	73.69	68.45	1509.39	52.90	43.99	48.89	541	61.72	43.98	73.97	68.33	69.14	86.41	51.46	56.17	89.56	55.57
	✗	✓	✓	54.07	74.02	66.82	1481.78	58.01	44.73	51.11	605	62.13	46.71	76.18	69.00	66.81	87.81	53.20	57.30	90.20	56.43
	✓	✓	✓	56.78	75.60	68.62	1512.50	59.35	46.33	52.01	639	63.93	50.24	75.55	70.33	69.82	89.09	55.60	58.04	91.23	57.87
CLIP	✗	✗	✗	51.51	68.64	64.36	1289.62	54.25	44.56	43.17	306	43.86	27.36	66.00	60.00	64.39	81.61	45.40	53.42	90.50	50.58
	✗	✓	✗	51.71	69.00	63.84	1335.01	53.71	41.72	44.14	310	48.69	34.99	69.93	62.00	63.38	80.77	45.82	53.36	89.82	51.40
	✗	✗	✓	51.54	68.98	64.98	1302.20	54.04	42.02	42.96	310	44.33	27.44	65.37	61.67	64.69	82.33	45.37	53.46	90.05	50.59
	✗	✓	✓	52.76	69.99	65.15	1327.62	53.59	42.89	44.78	313	48.77	35.76	69.75	63.00	64.46	82.20	45.50	53.73	90.66	51.99
	✓	✓	✓	54.77	69.93	65.20	1474.65	56.47	44.56	45.45	365	49.93	39.36	70.40	64.00	65.58	83.30	48.90	55.95	90.30	53.24

Table 13. Ablation study on loss functions.

\mathcal{G}_L	$+\mathcal{L}_{\text{MM}}$	$+\mathcal{L}_{\text{GA}}$	$+\mathcal{L}_{\text{CGA}}$	GQA	MMB ^{EN}	SEED ^I	MME	RWQA	MMMU	MM*	OCRB	TVQA	CQA	AI2D	MMVP	CV-B ^{2D}	SQA	MathV	Hallu	POPE	Avg.
SigLIP 2	✗	✗	✗	55.03	73.97	67.57	1510.73	53.86	44.78	49.06	536	62.06	43.52	73.74	69.00	67.87	86.51	52.20	56.05	90.90	55.72
	✓	✗	✗	55.02	71.97	64.59	1500.80	51.38	44.35	47.41	512	60.40	42.20	70.35	66.00	64.22	82.57	52.72	54.11	85.53	53.76
	✗	✓	✗	54.65	73.56	65.84	1456.21	58.97	45.21	52.09	617	63.07	49.07	72.26	67.67	68.94	85.93	55.89	55.91	89.49	56.46
	✓	✗	✓	56.78	75.60	68.62	1512.50	59.35	46.33	52.01	639	63.93	50.24	75.55	70.33	69.82	89.09	55.60	58.04	91.23	57.87
CLIP	✗	✗	✗	51.51	68.64	64.36	1289.62	54.25	44.56	43.17	306	43.86	27.36	66.00	60.00	64.39	81.61	45.40	53.42	90.50	50.58
	✓	✗	✗	48.48	66.08	63.93	1222.30	52.14	42.42	43.24	290	43.89	26.52	64.28	60.67	61.27	83.16	45.04	54.44	88.77	49.71
	✗	✓	✗	54.72	68.16	63.26	1431.67	53.80	43.78	44.78	359	49.14	37.83	70.67	64.67	65.68	79.36	46.46	53.91	86.98	52.01
	✓	✗	✓	54.77	69.93	65.20	1474.65	56.47	44.56	45.45	365	49.93	39.36	70.40	64.00	65.58	83.30	48.90	55.95	90.30	53.24

ROSS [112], we use SigLIP-ViT-SO400M/14@384 [126] to ensure fair evaluation. CLIP [94] is trained with contrastive loss for vision-language alignment. We adopt CLIP-ViT-L/14@336, which processes 336×336 images into 576 vision tokens. DINOv2 [97] leverages self-contrastive and self-distillation learning for visual feature extraction. We use DINOv2-Large/14@224, encoding 224×224 images into 384 vision tokens. AIMv2 [38] is a native-resolution encoder trained via autoregressive pixel-wise prediction with an auxiliary LLM backbone. We adopt AIMv2-Large/14, which patchifies images into 14×14 patches, with images resized to a maximum of 224×224 pixels. Qwen-ViT [8] serves as the native-resolution vision encoder in Qwen2.5-VL with patch size 14. We utilize the encoder from Qwen2.5-VL-7B-Instruct and set the maximum resolution to 512×512 pixels. **Encoder-free architecture.** To validate LaVer’s generalizability beyond traditional vision encoders, we adopt an encoder-free architecture [23, 30, 56]. We employ a 3-layer MLP with 3584 intermediate hidden dimensions to project images into visual tokens with patch size 16, supporting up to 512×512 pixels. During Stage 1, only the MLP is trained; in Stages 2 and 3, both the MLP projector and LLM backbone are jointly optimized.

Packed visual sequence. To improve training efficiency while maintaining independent visual reconstruction without interfering with multimodal sequence modeling, we pack vision tokens from multiple images into a single sequence, excluding their corresponding text tokens. Specifically, we construct diagonally blocked bidirectional attention and concatenated 2D-RoPE for the packed visual sequences. Across all vision encoders, we pack vision tokens from 2 images into a single sequence of length 2048 with padding tokens, yielding two separate visual sequences per

local batch on each GPU with batch size 4. The attention and positional embedding mechanisms for packed visual sequences are illustrated in Fig. 10.

Evaluation. We conduct comprehensive evaluation using the VLMEvalKit [35] toolbox. Our evaluation suite encompasses a diverse set of benchmarks: GQA [49] for compositional visual reasoning, MMBench (MMB^{EN}) [70] for comprehensive multimodal understanding, SEED-Image (SEED^I) [59] for generative comprehension, MME [39] for perception and cognition evaluation, RealWorldQA (RWQA) [25] for real-world visual question answering, MMMU [125] for massive multi-discipline understanding, MMStar (MM*) [20] for challenging multi-modal reasoning, OCR-Bench (OCRB) [71] for text recognition capabilities, TextVQA (TVQA) [98] for reading text in images, ChartQA (CQA) [78] for chart understanding, AI2D [53] for diagram comprehension, CV-Bench-2D (CV-B^{2D}) [102] for vision-centric capabilities, MMVP [103] for visual perception, ScienceQA (SQA) [75] for science question answering with explanations, MathVista (MathV) [76] for mathematical reasoning in visual contexts, HallucinationBench (Hallu) [44] for hallucination detection, and POPE [63] for object hallucination evaluation. We employ the default system prompt and instruction template for each benchmark to ensure fair comparison. For averaged results, we compute the mean value across all benchmarks, with MME and OCR-Bench normalized to the range [0.0, 1.0] to maintain consistent scaling.

For ReasonSeg [55] evaluation, we adopt the fine-tuning protocol established in [101]. Specifically, we initialize models using checkpoints from stage 2 for both the baseline and LaVer configurations. Following [101], we fine-tune the models to acquire sophisticated segmentation reasoning capabilities using a comprehensive dataset mixture com-

Table 14. **Language performance comparison.**

Benchmark	SigLIP 2			CLIP		
	Baseline	LaVer	Δ_{Baseline}	Baseline	LaVer	Δ_{Baseline}
IFEval	70.34	70.77	$\uparrow 0.43$	68.96	68.24	$\downarrow 0.72$
MMLU	56.52	57.48	$\uparrow 0.96$	58.34	58.67	$\uparrow 0.33$
BBH	33.25	32.96	$\downarrow 0.29$	34.78	34.93	$\uparrow 0.15$
Average	53.37	53.74	$\uparrow 0.37$	54.03	53.95	$\downarrow 0.08$

prising semantic segmentation datasets (COCOStuff [13], Mapillary [83], ADE20K [135], nuScenes [14]), referring segmentation datasets (RefCOCO [14], RefCOCO+ [14], RefCOCOg [14]), and the general VQA dataset LLaVA-665K [66], totaling approximately 4M samples. The detailed training configuration is presented in Table 6, with hyperparameters primarily adopted from [101].

Computational overhead analysis. The implementation of LaVer introduces additional computational overhead, primarily stemming from the forward passes required for both student and teacher models to process image tokens, as well as the EMA updates for the teacher model parameters. As detailed in Table 7, we conduct a comprehensive computational cost analysis focusing on stage 2, where LaVer is applied (stages 1 and 3 remain identical to the baseline). Across different vision encoders, LaVer incurs training time increases of 13-16% and memory consumption increases of 14-26% compared to the baseline. Specifically, with SigLIP 2 [106], training time increases from 8h 27min to 9h 34min, while memory consumption rises from 55.24 GB to 69.82 GB per GPU (averaged across 16 GPUs). Similar patterns are observed with CLIP [94] and DINOv2 [87] vision encoders. Despite these additional costs, the substantial performance improvements demonstrated across diverse benchmarks and architectural configurations justify this computational overhead, establishing LaVer as a practical and effective approach for enhancing MLLMs.

E. Visualization details

we provide the details about how the figures are generated in the paper.

Fig. 1. We present a comprehensive performance comparison between LaVer and the baseline across 17 benchmarks, utilizing SigLIP 2 [106] as the vision encoder and Qwen2.5-7B-Instruct [91] as the LLM backbone.

Fig. 2. (a) We randomly select an image from MMVP [103] and perform forward passes through both the baseline and LaVer models, extracting hidden states at different layers. Using SigLIP 2 [106] as the vision encoder and Qwen2.5-7B-Instruct [91] as the LLM backbone, we normalize the hidden states and compute feature-wise cosine similarity. The visualization reveals that vision tokens exhibit substantially higher inter-feature cosine similarity in the last layer compared to middle layers, demonstrating progressive visual representation homogenization. (b-

c) We extract the last-layer hidden states from both baseline and LaVer models and apply t-SNE [107] to project the high-dimensional features into 2D space. The scattered features are color-coded to distinguish vision and text tokens. Compared to the baseline, LaVer’s visual features exhibit stronger interaction with textual features, indicating more effective learning of joint multimodal embeddings. (d) We process images from MMVP [103] through both models and extract hidden states of vision tokens across all layers, computing the averaged cosine similarity between normalized features. For the baseline, the averaged visual cosine similarity decreases mildly in early and middle layers but increases drastically in deeper layers, indicating rapid visual information loss in the final stages. In contrast, LaVer maintains a consistent decreasing trend throughout all layers, preserving visual discriminability. (e) We analyze the proportion of attention allocated to vision tokens across layers, following [21, 56]. Specifically, using images and corresponding queries from MMVP [103], we compute the proportion of attention scores allocated to previous vision tokens for each predicted token. These layer-wise proportions are averaged across all predictions to reveal the overall trend. The comparison demonstrates that LaVer enables the model to allocate significantly more attention to vision tokens, indicating more effective utilization of visual representations.

Fig. 4. (a) We extract the hidden states of vision tokens from the last layer and reshape them to recover their spatial structure. Applying PCA [1] for dimensionality reduction to 3 components, we normalize the features to the range [0, 255] and visualize them as a 3-channel RGB image. The visualization demonstrates that LaVer generates highly discriminative visual features while preserving clear spatial structural information. All experiments use images from MMVP [103], SigLIP 2 [106] as the vision encoder, and Qwen2.5-7B-Instruct [91] as the LLM backbone. (b) We analyze the training dynamics of the baseline and models trained with different loss configurations. Specifically, using images from MMVP [103], we compute the averaged normalized cosine similarity of last-layer visual features at 1K iteration intervals. While naive application of MIM leads to visual feature inconsistency, LaVer effectively prevents the MIM shortcut, guiding the model toward more discriminative visual representations throughout training.

Fig. 6. We visualize the attention scores of the last predicted token on images from MMVP [103], alongside the corresponding PCA visualization of last-layer visual features. The results demonstrate that LaVer enhances the model’s ability to focus on spatially relevant regions that correspond to the generated text tokens, indicating improved visual-textual alignment.

Table 15. **Performance comparison with different LLM backbone.** LaVer achieves superior performance on Vicuna-7B-v1.5 [133], demonstrating its effectiveness and generalizability across diverse architectural configurations.

Benchmark	SigLIP 2			CLIP			DINOv2		
	Baseline	LaVer	Δ_{Baseline}	Baseline	LaVer	Δ_{Baseline}	Baseline	LaVer	Δ_{Baseline}
GQA	50.00	53.52	$\uparrow 3.52$	51.01	54.02	$\uparrow 3.01$	49.75	51.76	$\uparrow 2.01$
MMB ^{EN}	67.83	68.55	$\uparrow 0.72$	66.50	65.13	$\downarrow 1.37$	53.69	55.29	$\uparrow 1.60$
SEED ^I	66.33	67.29	$\uparrow 0.96$	64.58	65.36	$\uparrow 0.78$	60.09	63.77	$\uparrow 3.68$
MME	1426.52	1441.46	$\uparrow 14.94$	1292.78	1317.35	$\uparrow 24.57$	1232.67	1248.07	$\uparrow 15.40$
RWQA	55.42	58.43	$\uparrow 3.01$	53.86	55.56	$\uparrow 1.70$	45.75	48.55	$\uparrow 2.80$
MMMU	40.89	42.11	$\uparrow 1.22$	41.00	44.33	$\uparrow 3.33$	40.33	41.33	$\uparrow 1.00$
MM*	51.74	53.28	$\uparrow 1.54$	44.85	45.38	$\uparrow 0.53$	40.82	44.24	$\uparrow 3.42$
OCRB	389	401	$\uparrow 12$	311	352	$\uparrow 41$	306	349	$\uparrow 43$
TVQA	65.07	67.36	$\uparrow 2.29$	52.39	52.60	$\uparrow 0.21$	40.66	42.25	$\uparrow 1.59$
CQA	62.48	64.80	$\uparrow 2.32$	37.84	44.56	$\uparrow 6.72$	28.44	29.04	$\uparrow 0.60$
AI2D	70.84	72.68	$\uparrow 1.84$	67.97	69.09	$\uparrow 1.12$	61.14	63.09	$\uparrow 1.95$
MMVP	47.67	49.00	$\uparrow 1.33$	41.00	44.67	$\uparrow 3.67$	44.33	46.67	$\uparrow 2.34$
CV-B ^{2D}	54.19	56.55	$\uparrow 2.36$	42.94	44.45	$\uparrow 1.51$	41.47	45.49	$\uparrow 4.02$
SQA	73.89	75.08	$\uparrow 1.19$	70.79	70.37	$\downarrow 0.42$	62.93	65.33	$\uparrow 2.40$
MathV	54.20	56.80	$\uparrow 2.60$	43.90	46.40	$\uparrow 2.50$	40.80	43.30	$\uparrow 2.50$
Hallu	66.89	67.83	$\uparrow 0.94$	67.52	70.25	$\uparrow 2.73$	60.26	69.74	$\uparrow 9.48$
POPE	87.07	88.07	$\uparrow 1.00$	90.13	90.73	$\uparrow 0.60$	86.90	87.67	$\uparrow 0.77$
Average	53.85	55.43	$\uparrow 1.58$	49.24	50.81	$\uparrow 1.57$	44.60	46.96	$\uparrow 2.37$

Table 16. **Performance comparison of stage 2.** LaVer achieves superior performance on stage 2, indicating a direct effect of LaVer on visual representation enhancement.

Benchmark	SigLIP 2			CLIP			DINOv2		
	Baseline	LaVer	Δ_{Baseline}	Baseline	LaVer	Δ_{Baseline}	Baseline	LaVer	Δ_{Baseline}
GQA	52.03	53.77	$\uparrow 1.74$	50.25	53.28	$\uparrow 3.03$	48.01	51.26	$\uparrow 3.25$
MMB ^{EN}	70.51	73.52	$\uparrow 3.01$	67.04	67.53	$\uparrow 0.49$	57.82	60.77	$\uparrow 2.95$
SEED ^I	65.63	66.92	$\uparrow 1.29$	58.94	64.55	$\uparrow 5.61$	60.74	61.91	$\uparrow 1.17$
MME	1387.81	1434.21	$\uparrow 46.40$	1215.99	1313.32	$\uparrow 97.33$	1169.80	1224.12	$\uparrow 54.32$
RWQA	52.43	58.74	$\uparrow 6.31$	52.38	54.76	$\uparrow 2.38$	48.42	52.29	$\uparrow 3.87$
MMMU	42.67	44.67	$\uparrow 2.00$	42.44	42.89	$\uparrow 0.45$	40.22	41.67	$\uparrow 1.45$
MM*	45.11	51.41	$\uparrow 6.30$	41.63	44.25	$\uparrow 2.62$	39.43	41.10	$\uparrow 1.67$
OCRB	304	407	$\uparrow 103$	288	306	$\uparrow 18$	247	258	$\uparrow 11$
TVQA	54.94	59.99	$\uparrow 5.05$	60.92	62.35	$\uparrow 1.43$	52.44	54.97	$\uparrow 2.53$
CQA	51.60	54.16	$\uparrow 2.56$	40.40	46.80	$\uparrow 6.40$	40.40	41.20	$\uparrow 0.80$
AI2D	70.37	74.94	$\uparrow 4.57$	69.56	70.65	$\uparrow 1.09$	71.14	72.47	$\uparrow 1.33$
MMVP	38.33	43.67	$\uparrow 5.34$	26.00	37.00	$\uparrow 11.00$	26.67	28.00	$\uparrow 1.33$
CV-B ^{2D}	44.46	49.35	$\uparrow 4.89$	40.19	45.79	$\uparrow 5.60$	40.68	42.61	$\uparrow 1.93$
SQA	70.09	73.73	$\uparrow 3.64$	65.49	69.12	$\uparrow 3.63$	64.57	64.60	$\uparrow 0.03$
MathV	49.10	55.60	$\uparrow 6.50$	50.90	53.90	$\uparrow 3.00$	42.10	43.20	$\uparrow 1.10$
Hallu	56.15	59.62	$\uparrow 3.47$	56.38	58.31	$\uparrow 1.93$	55.10	57.05	$\uparrow 1.95$
POPE	85.90	85.67	$\downarrow 0.23$	89.77	90.83	$\uparrow 1.06$	88.13	88.87	$\uparrow 0.74$
Average	50.01	53.34	$\uparrow 3.33$	47.83	50.76	$\uparrow 2.93$	45.68	47.22	$\uparrow 1.54$

F. Additional Experiment Results

Full results of the parameter scaling property of LaVer.

Table 8 presents a comprehensive evaluation of LaVer’s scalability across different model parameter sizes, ranging from Qwen2.5-1.5B-Instruct to Qwen2.5-7B-Instruct [91], using both SigLIP 2 [106] and CLIP [94] vision encoders. The results demonstrate that LaVer consistently delivers performance improvements over the baseline across all parameter scales. For SigLIP 2-based models, LaVer achieves average improvements of **+2.42**, **+2.07**, and **+2.15** points for 1.5B, 3B, and 7B parameter configurations, respectively. Similarly, for CLIP-based models, LaVer yields average gains of **+3.12**, **+1.31**, and **+2.66** points across the same parameter scales. Notably, LaVer exhibits particularly strong improvements on challenging benchmarks such as OCR-Bench [71] (up to **+103** points for SigLIP 2-7B) and MME [39] (up to **+185.03** points for CLIP-

7B), ChartQA [78] (up to **+12.00** points for CLIP-7B), and MathVista [76] (up to **+7.20** points for SigLIP 2-1.5B). The consistent positive gains across 17 diverse benchmarks and multiple parameter scales substantiate that LaVer possesses robust scaling properties with respect to model parameters, maintaining its effectiveness in mitigating visual representation homogenization regardless of model capacity.

Full results of the data scaling property of LaVer.

Table 9 presents a comprehensive analysis of LaVer’s scalability across different training dataset sizes, ranging from 800K to 4M samples, using both SigLIP 2 [106] and CLIP [94] vision encoders with Qwen2.5-7B-Instruct [91] as the language model. The results demonstrate that LaVer consistently delivers substantial performance improvements over the baseline across all data scales. For SigLIP 2-based models, LaVer achieves average improvements of **+2.15**, **+2.16**, and **+1.80** points for 800K, 2M,

Table 17. **Compatibility of LaVer with enriched visual inputs.** LaVer consistently improves performance when combined with methods that enrich visual inputs, demonstrating its broad compatibility and effectiveness across diverse visual enhancement strategies.

\mathcal{G}_ϵ	GQA	MMB ^{EN}	SEED [†]	MME	RWQA	MMMU	MM*	OCRB	TVQA	CQA	AI2D	MMVP	CV-B ^{2D}	SQA	MathV	Hallu	POPE	Avg.
A-MoF	51.52	70.83	62.53	1312.14	54.77	41.11	41.53	338	59.46	41.04	73.45	41.67	61.34	67.31	51.20	62.47	89.13	51.19
A-MoF + LaVer	52.26	72.02	65.66	1321.51	56.34	43.22	43.87	360	61.68	42.52	78.38	44.67	62.66	68.51	54.40	62.89	89.57	52.92

and 4M training samples, respectively. Similarly, for CLIP-based models, LaVer yields progressively increasing average gains of **+2.66**, **+3.04**, and **+3.77** points across the same data scales, indicating enhanced effectiveness with larger training datasets. Notably, LaVer exhibits particularly strong improvements on challenging benchmarks such as TextVQA [98] (up to **+8.61** points for CLIP-2M). The consistent positive gains across 17 diverse benchmarks and multiple data scales substantiate that LaVer possesses robust scaling properties with respect to training data size, maintaining its effectiveness in mitigating visual representation homogenization regardless of dataset scale. Furthermore, the observation that CLIP-based models show increasing improvements with larger datasets (from **+2.66** to **+3.77**) suggests that LaVer’s benefits become more pronounced when trained on more extensive data, highlighting its potential for further performance gains with additional training data.

Full results of the ablation study on masking strategies. Table 10 presents a comprehensive analysis of LaVer’s performance under different masking strategies, examining both cosine and constant scheduling approaches across various masking ratios. The results are evaluated on 17 diverse benchmarks using SigLIP 2 [106] and CLIP [94] vision encoders with Qwen2.5-7B-Instruct [91] as the language model. For SigLIP 2-based models, the cosine scheduling strategy with a masking ratio of 0.05 achieves the best average performance of **57.87**, representing a substantial improvement of **+2.15** points over the baseline (55.72). This configuration demonstrates consistent gains across most benchmarks. Comparing scheduling strategies, cosine scheduling generally outperforms constant scheduling across different masking ratios. For instance, at a ratio of 0.05, cosine scheduling achieves **57.87** compared to constant scheduling’s **56.32**, demonstrating the effectiveness of gradually varying masking intensity during training. Regarding masking ratio selection, lower ratios (0.05-0.1) consistently yield superior performance compared to higher ratios (0.2-0.3) under cosine scheduling, suggesting that moderate masking preserves sufficient visual information while effectively mitigating representation homogenization. For CLIP-based models, similar trends emerge with cosine scheduling at 0.05 ratio achieving the best average performance of **53.24**, representing a **+2.66** point improvement over the baseline. The results demonstrate LaVer’s robustness across different masking configurations,

with the cosine scheduling strategy at lower masking ratios consistently delivering optimal performance across both vision encoders and diverse evaluation benchmarks. We hypothesize that the inferior performance observed with high masking ratios stems from insufficient convergence, as conventional MIM-based methods typically require large-scale training to fully develop the model’s reconstruction capabilities [17, 87, 97]. Scaling to larger datasets remains an avenue for future investigation.

Full results of the ablation study on EMA updating strategies. Table 11 presents a comprehensive analysis of LaVer’s performance under different EMA teacher updating strategies, evaluated across diverse benchmarks using SigLIP 2 [106] and CLIP [94] vision encoders with Qwen2.5-7B-Instruct [91] as the LLM backbone. The results demonstrate LaVer’s robustness across various EMA configurations, with cosine scheduling slightly outperforming constant scheduling. Regarding updating frequency, moderate frequencies (50-200 steps) generally yield optimal performance, with 100 steps emerging as the most balanced configuration across both vision encoders. For decay rate selection, a rate of 0.95 demonstrates superior stability and performance compared to both lower (0.9) and higher (0.99, 0.999) rates. The comprehensive evaluation across diverse benchmarks confirms that LaVer’s performance remains consistently strong regardless of the specific EMA strategy employed, highlighting the method’s robustness and effectiveness in learning intrinsic visual representation capabilities.

Full results of the ablation study on spatial awareness. Table 12 presents a comprehensive analysis of LaVer’s spatial awareness mechanisms, evaluated across diverse benchmarks. The results reveal several key insights. First, employing mixed attention alone (full attention for vision tokens) yields moderate improvements over the baseline, demonstrating that enhanced token interactions can benefit visual understanding. Second, applying 2D-RoPE in isolation shows minimal impact, with performance remaining largely comparable to the baseline. Third, combining mixed attention with 2D-RoPE without LaVer produces mixed results, with performance gains that are inconsistent across benchmarks. Most importantly, the full LaVer framework, which integrates all three components achieves the best overall performance. This configuration demonstrates consistent improvements across challenging benchmarks. These results confirm that LaVer’s holistic ap-

proach to spatial awareness, combining learned visual representations with architectural enhancements, is essential for achieving superior multimodal understanding capabilities.

Full results of the ablation study on loss components.

Table 13 provides a comprehensive analysis of different loss function configurations in LaVer, evaluated across diverse benchmarks. The results reveal three critical insights into the design of effective visual representation learning objectives. First, applying masked image modeling (\mathcal{L}_{MIM}) alone significantly degrades performance, with average scores dropping from **55.72** to **53.76** for SigLIP 2 and from **50.58** to **49.71** for CLIP. This deterioration stems from the *visual feature inconsistency* problem, where the model exploits the MIM objective by generating identical visual features, thereby undermining the discriminative capacity essential for downstream tasks. Second, incorporating the global alignment loss (\mathcal{L}_{GA}) alongside \mathcal{L}_{MIM} partially mitigates this issue, improving average performance to **56.46** for SigLIP 2 and **52.01** for CLIP. However, this configuration still underperforms the full LaVer framework, as the symmetric nature of \mathcal{L}_{GA} constrains the model’s ability to learn sufficiently discriminative representations. Third, our proposed contrastive global alignment loss (\mathcal{L}_{CGA}) effectively addresses both shortcomings, achieving the best overall performance with average scores of **57.87** for SigLIP 2 and **53.24** for CLIP. These results confirm that \mathcal{L}_{CGA} simultaneously prevents visual feature inconsistency while encouraging discriminative feature learning, thereby enhancing both visual information preservation and utilization across diverse multimodal understanding tasks.

Language capabilities. A potential concern when introducing vision-centric supervisory signals is whether they may compromise the model’s language capabilities. To address this, we evaluate the language performance of both the baseline and our LaVer model using SigLIP 2 [106] and CLIP [94] as vision encoders, respectively, as shown in Table 14. Specifically, we adopt three representative benchmarks: IFEval [137], which evaluates the model’s capability to strictly follow instructions; MMLU [47], a comprehensive general language benchmark containing diverse tasks across various domains; and BBH [100], which assesses language reasoning and world knowledge capabilities. The results demonstrate that LaVer maintains competitive language performance across both vision encoder configurations. These findings confirm that LaVer successfully preserves language capabilities while simultaneously achieving substantial improvements in visual understanding tasks, thereby validating the effectiveness of our approach in balancing multimodal learning objectives.

Extended comparison with different LLM backbone.

To validate the generalizability of LaVer across different architectural configurations, we conduct comprehensive ex-

periments using Vicuna-7B-v1.5 [133] as the LLM backbone, paired with three vision encoders: SigLIP 2 [106], CLIP [94], and DINOv2 [87]. As shown in Table 15, LaVer consistently outperforms the baseline across all three vision encoder configurations, achieving average improvements of **+1.58**, **+1.57**, and **+2.37** points for SigLIP 2, CLIP, and DINOv2, respectively. Notably, LaVer demonstrates substantial gains on benchmarks requiring fine-grained visual understanding, including ChartQA [78] (**+2.32**, **+6.72**, **+0.60**), MMVP [103] (**+1.33**, **+3.67**, **+2.34**), and CV-Bench-2D [102] (**+2.36**, **+1.51**, **+4.02**). These results confirm that LaVer effectively preserves and enhances multimodal capabilities across different LLM architectures, demonstrating its robustness and broad applicability in diverse scenarios.

Performance comparison of stage 2. Following the state-of-the-art open-source framework LLaVA-OneVision [3], we adopt a 3-stage training recipe and exclusively apply LaVer to stage 2, which is responsible for visual knowledge injection. To thoroughly investigate how LaVer facilitates visual knowledge learning, we compare models with and without LaVer during stage 2, using three vision encoders: SigLIP 2 [106], CLIP [94], and DINOv2 [87]. As presented in Table 16, LaVer consistently demonstrates substantial improvements across all configurations, achieving average gains of **+3.33**, **+2.93**, and **+1.54** points for SigLIP 2, CLIP, and DINOv2, respectively. Notably, LaVer exhibits particularly strong performance on benchmarks requiring fine-grained visual understanding: MMVP [103] shows remarkable improvements of **+5.34**, **+11.00** across the three encoders. These results reveal that the performance gains observed in stage 2 are even more pronounced than in the final stage, indicating that LaVer fundamentally enhances the model’s capacity to learn representative visual features during the critical visual knowledge injection phase, thereby establishing a strong foundation for superior multimodal performance across diverse downstream tasks.

Compatibility with other methods. LaVer introduces vision-centric supervisory signals by predicting masked vision tokens, a design that naturally ensures compatibility with methods that enrich visual inputs. To validate this compatibility, we integrate LaVer with A-MoF [103], which aggregates visual features from multiple vision encoders to form more informative visual embeddings. Specifically, following [103], we combine visual features from CLIP-ViT-L/14@224 [94] and DINOv2-Large/14@224 [87] with balance coefficients of 0.25, 0.75, which are empirically validated as optimal hyperparameters in [103]. The identical patch size and resolution ensure that visual features share the same shape and can be directly aggregated. As presented in Table 17, LaVer consistently delivers substantial improvements across all benchmarks when integrated with



Figure 11. Qualitative comparisons on MMVP [103].

A-MoF. Overall, LaVer achieves an average improvement of **+1.73** points across all benchmarks, demonstrating that it provides additional benefits when integrated with vision-enhanced methods and confirming its broad compatibility with diverse visual enhancement strategies.

G. Qualitative Analysis

We provide additional qualitative comparisons in Fig. 11 on MMVP [103]. As illustrated in Fig. 11, we visualize both the attention scores on vision tokens from the last predicted token and the PCA visualization of visual features extracted from the final layer. The baseline model frequently fails to attend to spatial regions that are semantically relevant

to the text query, exhibiting limited attention distributions across the visual input. In contrast, our LaVer consistently allocates substantially higher attention weights to the corresponding regions of interest, thereby enabling more accurate and contextually appropriate responses. Furthermore, LaVer demonstrates the ability to capture diverse visual patterns and generate highly discriminative visual features that encode rich structural information. These qualitative results provide compelling evidence that LaVer effectively mitigates modality imbalance by incorporating visual supervisory signals, enabling the model to integrate visual and textual modalities seamlessly and achieve superior performance on multimodal tasks.